SENSUM

SENSUM

Framework to integrate Space-based and in-situ sENSing for dynamic vUlnerability and recovery Monitoring

FP7-SPACE-2012-1 Collaborative Project **312972**

Deliverable

Deliverable	Present day and future remote sensing data. Report on globally available present-day and future remote sensing data and products.
D2.1	

Workpackage	WP2	**Status (F=Final, D=Draft)**	F
File name	Present_and_future_RS_data_final		
Dissemination Level (PU=Public; RE=Restricted; CO=Confidential)		CO	

Document Control Page

Version	Date	Comments
1	16/06/2013	First Draft (internal revision)
2	18/06/2013	Second Draft (internal revision)
3	19/06/2013	Third Draft (for external revision)
4	23/06/2013	First External Revision (Marc Wieland)
5	26/06/2013	Fourth draft (for final external revision)
6	02/07/2013	Final review by project management
7	16/07/2013	Final report

Authors	
Name	**Institution**
Dr Hannes Taubenböck	DLR-DFD
Christian Geiß	DLR-DFD
Martin Klotz	DLR-DFD

Deliverable Leader	**Name**	Dr Hannes Taubenböck
	Institution	DLR-DFD
Keywords	Remote sensing, Future missions, Sensors, Global urban maps, Sentinel, Vulnerability, Hazard	

Table of Contents

Index of Tables

Illustration Index

Glossary of Terms

GFZ	German Research Centre for Geosciences, DE
ALOS	Advanced Land Observing Satellite
CAIAG	Central Asian Institute for Applied Geosciences, KG
CLC	CORINE Land Cover
CLC00	CORINE Land Cover 2000
CSA	Canadian Space Agency
DEM	Digital Elevation Model
DESDynI	Deformation, Ecosystem Structure and Dynamics of Ice

D-InSAR	Differential Interferometric Synthetic Aperture Radar
DLR	German Aerospace Centre, DE
DLR-ZKI	Centre for Satellite Based Crisis Information of the German Aerospace Centre, DE
DMSP	Defence Meteorological Satellite Program
DoW	Description of Work
DSM	Digital Surface Model
EC	European Commission
EEA	European Environment Agency
EnMAP	Environmental Mapping and Analysis Program
ESA	European Space Agency
ETM+	Enhanced Thematic Mapper
EUCENTRE	European Centre for Training and Research in Earthquake Engineering, IT
FOR	Field of regard, i.e. the area covered for a sensor's detector pointing to all mechanically possible directions
GED	Global Exposure Database
GED4GEM	Global Exposure Database for the Global Earthquake Model
GEM	Global Earthquake Model
GHSL	Global Human Settlement Layer
GLOBC	GlobCover
GMES	Global Monitoring for Environment and Security
GRUMP	Global Rural-Urban Mapping Project
HR	High Resolution (reffereing to the GMES classes HR1 and HR2)
HR1	High Resolution according to GMES (2011): 4-10m

HR2	High Resolution according to GMES (2011): 10-30m
HSI	Hyperspectral Imager
Hyperspectral	Capability of a sensor system to acquire imagery in multiple contiguous (>100) spectral bands
HYDE3	History Database of the Global Environment
HyspIRI	Hyperspectral Infrared Imager
ICAT	ImageCat Ltd., UK
IGEES	Institute for Geology and Earthquake Engineering, TJ
IMPSA	Impervious Surface Area
InSAR	Interferometric Synthetic Aperture Radar
IS	Impervious Surface; surfaces impenetrable by water as such as sidewalks, driveways, rooftops and parking lots as indicator for urban functional land use
ISRO	Indian Space Research Organisation
JAXA	Japan Aerospace Exploration Agency
JRC	Joint Research Centre of the European Union
LIDAR	Light Detection And Ranging
LITES	DMSP-OLDS Nighttime Lights
LR	Low Resolution according to GMES (2011): >300m
LSCAN	Landscan
MOD500	MODIS Urban Land Cover 500m
MR	Medium Resolution (referring to the GMES classes MR1 and MR2)
MR1	Medium Resolution according to GMES (2011): 30-100m
MR2	Medium Resolution according to GMES (2011): 100-300m
MSS	Multispectral Scanner

Multispectral	Capability of a sensor system to acquire imagery in multiple (>1; <10) spectral bands
NASA	National Aeronautics and Space Administration
NGI	Norwegian Geotechnical Institute, NO
OLI	Operational Land Imager
OLS	Operation Linescan System
OSM	Open StreetMap
PAN	Panchromatic
Rural	Geographic area that is located outside cities and towns and comprises all population, housing, and territory not included by an urban area.
SAR	Synthetic Aperture Radar
SRTM	Shuttle Radar Topography Mission
Spotlight	Acquisition mode of the German radar sensor TerraSAR-X of 1m geometric resolution and 10km swath width
Stripmap	Acquisition mode of the German radar sensor TerraSAR-X of 3m geometric resolution and 30km swath width
Superspectral	Capability of a sensor system to acquire imagery in multiple (≥10) spectral bands
SWIR	Shortwave Infrared
TDL	TanDEM-L
TDS	TanDEM-X
TIRS	Thermal Infrared Sensor
TM	Thematic Mapper
TOPS	Terrain Observation by Progressive Scan
TSX	TerraSAR-X
Urban area	Characterised by high population densities and human

	features in comparison to areas surrounding it. Urban areas may be cities, towns or conurbations; however, the term is not commonly extended to rural settlements.
Urban functional area	defined in terms of the areas for which it provides services and facilities — the functional *area* (thus it may also include the countryside or free-standing settlements)
UCAM	University of Cambridge, UK
USGS	United States Geological Survey
VHR	Very High Resolution (referring to the GMES classes VHR1 and VHR2)
VHR1	Very High Resolution according to GMES (2011): <=1m
VHR2	Very High Resolution according to GMES (2011): 1-4m
VMAP0	Vector Map Level 0
VNIR	Visible to Near-Infrared
WP	Workpackage

Acknowledgement

The research leading to these results was supported by funding from the European Community's Seventh Framework Programme [FP7/2007-2013] under grant agreement n° 312972 "Framework to integrate Space-based and in-situ sENSing for dynamic vUlnerability and recover Monitoring".

Executive Summary

In terms of an integrative and comprehensive risk analysis, the issue of an appropriate data collection is widely recognized. In this context, remote sensing is generally perceived as a promising tool for an economical, up-to-date and independent data collection and has been employed in various investigations in the geo-risk context. A review of past applications reveals the versatility of remote sensing data and techniques with regard to the analysis of earthquake and landslide risks.

The study of earthquake hazard components reach from geologic site characterisations and fault mapping, detection of pre-event surface temperature anomalies for early warning, kinematics and dynamics of active fault systems, to the detection of earthquake-induced changes to the land surface. For landslides, remote sensing techniques and applications contribute to basic terrain analysis including monitoring of slope stability and land cover, the detection and mapping of pre-event landslide-related activities such as slow mass movements as well as the volumetric quantification of landslide related changes to land cover and form.

Remote sensing for vulnerability-centred investigations is a less long established field of research. Nevertheless, a vast amount of research aims at the derivation of pre-event vulnerability indicators – related to physical, demographic and socioeconomic aspects of vulnerability–. Also work on post-event emergency response and damage assessment employing especially very high resolution data has been carried out.

In the context of geo-risk analysis, both for pre- and post-event as well as hazard- and vulnerability-centred investigations, past- and present-day remote sensing missions have proven useful. Data with a coarser geometric resolution and larger spatial coverage per scene are able to contribute to overall evaluation of pre- and post-event situations. In contrast, it is yet both difficult and expensive to obtain high geometric resolution data such as airborne LIDAR or VHR optical data over larger areas affected, specifically in case of an earthquake event. In addition to that, the geometric resolution of the sensors and the associated scene size and thus, the spatial scale of analysis, need always be selected in consideration of the context of the objects to be analysed.

Future earth observation missions have the potential to play a key role in earthquake- and landslide-related investigations and to continue or even improve geoinformation products. For example, the ESA Sentinel missions will feature enhanced geometric and thematic capabilities and increased revisit capabilities at low cost. Other future missions such as ALOS-2, the RADARSAT constellation, DESDynI, CARTOSAT-3, ALOS-3, TerraSAR-X 2, TanDEM-L, WorldView-3, or the hyperspectral sensors EnMAP and HyspIRI still need to be assessed in terms of cost and applicability with respect to the particular research questions addressed. For example, TanDEM-L will open up opportunities to better understand the earth’s dynamic surface processes enabling continuous monitoring of earth surface deformation e.g. due to seismic movements, volcanic eruptions, landslides, subsidence or uplift in the range of centimetres. In this context, the enhanced capabilities of the described missions are believed to enable a leap forward in earthquake and landslide risk research both for hazard- as well as vulnerability-related investigations.

Apart from the future perspective, international research groups from both government and academia have produced remote sensing based geo-products in past years that will provide valuable input to vulnerability-related research in the context of this project. These include on the one hand large area global or regional land cover datasets that can be used as a first approximation of human and physical exposure as well as for the disaggregation of population census data. However, with regard to these products, a better understanding of each data set's strength and weakness is still on demand. On the other hand, space-based pre-operational emergency response services have produced a large product portfolio and significant experiences in post-event mapping applications in recent years.

Overall, from a technical perspective, the constantly increasing availability and accessibility of modern-day remote sensing technologies and the enhanced technical capabilities of future missions will provide new opportunities and data continuity for a wide range of geo-risk investigations. However, still today and in the future, data cost will be the main limiting factor.

1. Introduction: Capabilities of remote sensing for geo-risk analysis

Severe geo-physical hazards become natural disasters, i.e. destroy people's lives and livelihoods, every year. In terms of an integrative and comprehensive risk analysis, the issue of an appropriate data collection is widely recognized (Birkmann, 2006; Ehrlich et al., 2010; Geiß & Taubenböck, 2012). In this context, remote sensing is generally perceived as a promising tool for an economical, up-to-date and independent data collection (Dech, 1997; Mueller et al., 2006, Chiroiu et al., 2006; Esch et al., 2009; Guo, 2010). With regard to geo-risk research in particular, remote sensing is widely utilized as a contributing tool for hazard-related analysis (e.g. Fu et al., 2004; Stramando et al., 2005; Philip, 2010) as well as vulnerability-centred assessments (e.g. Taubenböck et al., 2008, 2009; Ehrlich et al., 2010; Deichmann et al., 2011).

This brief introduction highlights the capabilities of remote sensing systems and associated datasets with regard to particular applications in each phase of the disaster management cycle (Mileti 1999; Lindell, 2000; Tierney et al., 2001; Cartwright, 2005; Paul, 2011), i.e. (a) pre-event reduction (mitigation) and readiness (preparedness) as well as (b) post-event response and recovery with regard to both hazard- (*section 1.1*) and vulnerability-related (*section 1.2*) investigations.

With regard to the project at hand, the focus will be on applications that are related to the hazard types under study, namely earthquakes and landslides, which represent often a secondary effect of earthquakes, and the presentation of the particular sensor groups and associated datasets used. Subsequently, *chapter 2* will give an overview and exemplification of past- and present-day remote sensing missions with regard to particular spatial scales of analysis for vulnerability-related applications. *Chapter 3* reviews promising future missions that could be employed for remote sensing-based geo-risk research in future studies. Finally, *chapter 4* provides a summary of geo-products developed in the geo-risk context including land cover databases which enable the quantification of elements at risk. Beyond that, space-based pre-operational emergency response services are presented that have generated important experiences in the generation of disaster preparedness and response products.

Throughout the remaining report, applications, sensor groups and associated data sets will be related to the particular spatial scale of analysis at which they can be employed, mainly depending on the sensor-specific geometric resolution. The original categorization of the spatial scale of analysis developed by Geiß and Taubenböck (2012) is based on the scheme presented by Neer (1999) and includes a range of five classes, namely "very high resolution" (consisting of classes "extremely high resolution", "super-high resolution" and "very high resolution"), "high resolution", "medium resolution", "coarse resolution" and "very coarse resolution" (consisting of the classes "very coarse resolution" and "extremely coarse resolution"). However, as project SENSUM is closely linked to other projects and products of the European Union's Global Monitoring for Environment and Security programme (GMES) (GMES, 2012) the categorization was adapted to the classes of geometric resolution suggested by GMES

(2011) (Table 1.). Although the two schemes use different thresholds a generally correct harmonization was achieved.

Tab. 1 Categorization of spatial scales of analysis with regard to sensor-specific geometric resolution (Neer, 1999; GMES, 2011) (The dotted lines indicate the harmonization of both classification schemes with regard to the spatial scale of analysis)

Spatial scale of analysis	Neer (1999)		GMES (2011)	
	Geometric resolution (m)	*Nomenclature*	*Geometric resolution (m)*	*Nomenclature*
Focal	0.05-0.25	Extremely high resolution	<=1	Very high resolution 1 (VHR1)
	0.25-0.5	Super highresolution	1-4	Very high resolution 2 (VHR2)
	0.05-1.0	Very high resolution	4-10	High resolution 1 (HR1)
	1-4	High resoltion	10-30	High resolution 2 (HR2)
Local	4-12	Medium resolution	30-100	Medium resolution 1 (MR1)
Regional	12-50	Coarse resolution	100-300	Medium resolution 2 (MR2)
National	50-250	Very coarse resolution	>300	Low resolution (LR)
	>250	Extremely coarse resolution		

Today, there a many kinds of remote sensing systems: Optical sensors (by which also multi- and hyperspectral sensors are meant in the following), radar systems such as Synthetic Aperture Radar (SAR), as well as light detection and ranging (LIDAR) are the main systems used in the majority of remote sensing-based investigations on landslide and earthquake risk.

Optical sensors make use of the visible, near-infrared and short-wave infrared wavelength regions. These sensors produce imagery of the earth's surface by the passive detection of the solar radiation reflected from ground targets (Jensen, 2007). As different materials feature different reflection and absorption characteristics at different wavelengths, targets can be distinguished by their particular spectral reflectance signatures in the remotely sensed images. Depending on the number of spectral band in which the sensor is measuring, optical remote sensing systems can be classified into the following types according to CRISP (2001): (1) Panchromatic (PAN) sensors use a single channel mostly sensitive in the visible wavelength range and thus producing in essence black-and-white photographs of the earth. In the context of stereo visioning techniques these data are frequently used for generation of highly detailed digital elevation information. (2) Multispectral systems have a few spectral bands with each of these being sensitive in a narrow wavelength region. Resulting imagery contains multiple layers with both brightness and spectral (colour) information of the ground targets. One of the most prominent examples of this sensor group is carried by the United States' Landsat series of sensors (Fig. 1). Superspectral sensors are in essence very similar but feature a larger number of spectral bands, typically more than 10. (3) Finally, hyperspectral sensors, also known as imaging spectrometers monitor the earth's surface in about a hundred or more contiguous spectral bands, thus enabling a very precise spectral characterization of surface elements and materials.

Radar is the best known active sensor system and uses microwave radiation with wavelengths between one millimetre and one meter (Chuvieco & Huete, 2008). In contrast to optical sensors, these active systems emit microwave radiation to the earth's surface with an antenna, the so-called Synthetic Aperture. The reflected radiation is received at the sensor in different bands and polarisations. Using

wavelengths beyond the visual light, radar sensors are able to take images at any time of day and night and without disturbance of atmospheric influences, such as clouds. Furthermore, microwave radiation can penetrate the earth's surface and therefore explore the composition of surfaces. From the resulting imagery multiple information can be derived such as backscattering intensity or surface roughness. A prominent example for radar sensors is the German mission TerraSAR-X. Techniques of interferometric SAR or InSAR further enable precise measurement of the coherent radiation travel paths as a function of the satellite position and time of acquisition, thus, allowing for the generation of digital elevation models and measurement of centimetric surface deformations of the terrain (Jensen, 2007).

A further active remote sensing system is light detection and ranging (LIDAR) which is based on the airborne scanning of the earth surface by a near-infrared pulsed laser to measure ranges (variable distances) to the earth. These light pulses generate precise, three-dimensional information about the shape of the Earth and its surface characteristics (Mensah, 2009). The reflection of the laser from the target is detected and analyzed by receivers in the sensor. These record the precise time shift between the outgoing and incoming laser pulse to calculate the range distance between the sensor and the target. Combined with the positional parameters of the aircraft, these distance measurements are transformed to measurements of actual three-dimensional points of the reflective target in object space (Jensen, 2007).

Digital elevation information is crucial for investigation of landslide and earthquake risk and can be derived from each of the three sensor groups introduced, i.e. by indirect teachniques such as stereo imaging from optical data and SAR interferometry or directly from LIDAR measurements. Digital surface models (DSMs) belong to the group of digital elevation models (DEMs) which are defined as continuous representations of surface elevation (Miller, 20004). In this context, DSMs present the earth's surface including all features of the landscape such as vegetation and artificial objects, whereas digital terrain models (DTMs) are a representation of the bare-earth surface (Jensen, 2007).

Fig. 1 Radar intensity image (left) and optical natural colour image (right) of the Elbe river, Germany, acquired by TerraSAR-X and Landsat-5, respectively (source: DFD data repository)

1.1 Hazard parameters

Since the 1970s and the appearance of the first commercially available satellite-based sensor systems, remote sensing has evolved to a tool to actively map earthquake and landslide hazard components based on a wide range of data sets with differing capabilities (Tronin, 2006). The study of earthquake hazard components reach from geologic site characterisations and fault mapping, detection of pre-event surface temperature anomalies, kinematics and dynamics of active fault systems, to the detection of earthquake-induced changes to the land surface. For landslides, remote sensing techniques and applications contribute to basic terrain analysis including monitoring of slope stability and land cover, the detection and mapping of pre-event landslide-related activities as well as the volumetric quantification of landslide-related mass-movements and associated changes to land cover and form (Tralli et al., 2005). In this context, remote sensing has its share in both the pre- and post-event phase of the disaster management cycle. Overviews of the main remote sensing applications for both hazard types are listed in tables 1 and 2 with regard to the particular sensor group and datasets utilized.

(a) Remote sensing data and techniques are capable to support various components of **pre-event** hazard analysis due it its wide-spread availability, frequency of update and cost. A vast part of applications relate to quantitative observations such as the monitoring of geomorphologic land forms, land cover and tectonic features (Philip, 2010) as well as the generation of geologic, seismic and soil map products (Deichmann et al., 2011). In this context, digital surface models (DSMs) derived from LIDAR or SAR and optical stereophotogrammetric acquisitions present a suitable data basis for detailed and spatially consistent site characterizations. In this manner, several authors have studied landforms and geomorphologic inventories of hazard-prone regions by the extraction of geomorphologic and topographic features (e.g. Theilen-Willige, 2010). Furthermore, very high resolution (VHR1-2) digital elevation models derived from airborne LIDAR acquisitions allow for a particularly detailed mapping of faults with high accuracies (Cunningham et al., 2006). Other studies incorporate digital elevation models (DEMs) with additional multi-spectral medium to very high resolution (MR1 to VHR1) optical data for the extraction of geomorphometric and topographic parameters and terrain analysis such as the investigations of tectonic lineaments (Reif et al., 2011; Shafique et al., 2011). Pre-seismic surface deformations resulting from faulting can be mapped using concepts and techniques of differential interferometric SAR (D-InSAR) based on the phase difference of multi-temporal radar observations (e.g. Rott & Nagler, 2006). This technique is advantageous to GPS-measurements in terms of cost of acquisition and coverage and has contributed to various investigations such as the estimation of earthquake source parameters (Weston et al., 2012), the calculation of segment slip rates (Ding & Huang, 2011) and the quantification of aseismic strains between earthquake events (Fielding et al., 2004). Finally, thermal sensors are used for the detection of surface temperature anomalies that were observed prior to some events, what may hold information for earthquake prediction (Joyce et al., 2009a, Tronin, 2010).

Regarding landslide investigations, the combination of medium to very high resolution (MR1 to VHR1) optical data and high to very high resolution (HR2 to VHR1) digital elevation data present a promising data basis (Joyce et al., 2009a) allowing for a detailed terrain analysis such as the mapping of soils, land cover, land form as well as prediction of factors in space and time causing slope failures (e. g. Mantovani, 1996). For the monitoring of pre-event landslide activities, i.e. mass movements of slow moving landslides in the range of centimetres, concepts and techniques of D-InSAR are widely accepted as best practice (Joyce et al., 2009a).

(b) In the **post-event** phase remote sensing applications are mainly linked to the identification and quantification of hazard-induced changes to the land surface. Herein, the main focus is on the monitoring of surface deformations and displacements produced in the aftermath of earthquakes. In this regard, D-InSAR is also considered as the most suitable technique to monitor post-seismic deformations by the calculation of the phase difference between SAR images with a high temporal resolution (Masonett & Feigl, 1998). As InSAR provides very accurate results within a distance of a few kilometres from the fault but lacks consistent deformation information in the proximity of the fault zone, the use of medium to very high resolution (VHR1 to MR1) optical data can be complementary (Tronin, 2010).

With regard to landslide dynamics, optical data provides the most suitable data basis for multi-temporal image analysis employing various classification and change detection methods as presented by e.g. Joyce et al. (2009a). For example, Martha et al. (2011) as well as Stumpf and Kerle (2011) propose object-oriented image analysis approaches for the detection of landslides and the generation of landslide inventories by the use of shape, colour and texture feature from very high and resolution (VHR1 to HR1) optical data. By contrast, SAR features limitations owing to spatial resolution, sensor look angle, and the fact that there is no distinct backscatter signature associated with the mixed targets in a landslide body. However, it provides a viable option to optical data in case of cloud cover prevents optical acquisition. A further method commonly applied for landslide detection and monitoring is DEM differencing for volumetric quantification of landslide-related mass movements (e.g. Kaab, 2002; Ostir et al., 2003; Tsutsui et al., 2007). However, this technique is only useful for large landslides with a considerable vertical and volumetric dimension of changes. In this context, very high resolution (VHR1) panchromatic optical stereo sensors can produce highly detailed surface models as a cost-effective alternative compared to LIDAR acquisition.

Tab. 2 Earthquake hazard-related remote sensing applications and associated sensor groups / datasets (summarized from Joyce et al., 2009a; Geiß & Taubenböck, 2012; bold formatting indicates when a sensor group / associated data set has been identified as being advantageous compared to others mentioned)

<table>
<tr><th colspan="4">Hazard-related applications: Earthquake</th></tr>
<tr><th>Pre-event application</th><th>Contributing sensor group / associated datasets</th><th>Post-event application</th><th>Contributing sensor group / associated datasets</th></tr>
<tr><td>Site characterization: Mapping of geology, soils, land cover, landforms, seismic & tectonic features</td><td rowspan="2">Multispectral VHR1-MR1
DEM / DSM VHR1-MR1</td><td>Earthquake-induced change detection:
- Lineament analysis
- Suface deformation mapping
- Elevation displacement mapping</td><td>SAR / D-InSAR
Multispectral VHR1-MR1</td></tr>
<tr><td>Medium and small-scale fault mapping</td><td colspan="2" rowspan="5"></td></tr>
<tr><td>Measurement of pre-seismic faulting and surface deformations</td><td rowspan="4">SAR / D-InSAR
DEM / DSM VHR1-2 (LIDAR)</td></tr>
<tr><td>Estimation of earthquake source parameters</td></tr>
<tr><td>Calculation of slip rates</td></tr>
<tr><td>Quantification of aseimsic strains between events</td></tr>
<tr><td>Identification of precursor temperature anomalies</td><td>Thermal sensors</td><td colspan="2"></td></tr>
</table>

GMES (2011): VHR1: <= 1m; VHR2: 1-4m; HR1: 4-10m; HR2: 10-30m; MR1: 30-100; MR2: 100-300; LR: >300m

Tab. 3 Landslide hazard related remote sensing applications and associated sensor groups / datasets (summarized from van Westen et al., 2008; Joyce et al., 2009a; Geiß & Taubenböck, 2012; bold formatting indicates when a sensor group / associated data set has been identified as being advantageous compared to others mentioned)

<table>
<tr><th colspan="4">Hazard-related applications: Landslide</th></tr>
<tr><th>Pre-event application</th><th>Contributing sensor group / associated datasets</th><th>Post-event application</th><th>Contributing sensor group / associated datasets</th></tr>
<tr><td>Terrain analysis: Mapping soils, land cover, land forms, slope stability</td><td>Multispectral VHR1-MR1
DEM / DSM VHR1-HR2</td><td>Identification of landslide locations and extent</td><td>Multispectral VHR1-MR1
DEM / DSM VHR1-HR2
SAR</td></tr>
<tr><td>Measruement of velocity and extent of slow moving landslides</td><td rowspan="2">SAR / D-InSAR
Multispectral VHR1-HR1</td><td>Landslide-induced change detection:
- land cover / form</td><td rowspan="2">SAR / D-InSAR
DEM / DSM VHR1-MR1</td></tr>
<tr><td>Calculation of segment slip rates</td><td>Volumetric quantification of landslide related earth movement</td></tr>
</table>

GMES (2011): VHR1: <= 1m; VHR2: 1-4m; HR1: 4-10m; HR2: 10-30m; MR1: 30-100; MR2: 100-300; LR: >300m

1.2 Vulnerability parameters

An international widespread definition of vulnerability in the context of risk research describes vulnerability as ‘‘the conditions determined by physical, social, economic and environmental factors or processes, which increase the susceptibility of a community to the impact of a hazard’’ (UN/ISDR 2004). In this context, Bohle (2001) emphasizes the double structure of vulnerability with an external and internal side, where the external side includes the exposure to potentially damaging events, and the internal side relates to the capacity to cope with, resist and recover from the impact of a hazard. While coping capacity is the ability to cope with or adapt to hazard stress as a product of planned

preparation, spontaneous adjustments as well as relief and reconstruction made in response to the hazard (Taubenböck et al., 2008), exposure refers to the inventory of elements in an area in which hazard events may occur (UN/ISDR, 2004). Thus, if population (demographic vulnerability) or economic resources (economic vulnerability) were not located in (exposed to) hazard-prone areas, disaster risk would inexistent.

Remote sensing for vulnerability-centred investigations is a less long established field of research compared to hazard analysis and most of the past studies either only deal with the overall evaluation of the capabilities of remote sensing (e.g. Taubenböck et al., 2008) or explicitly address individual vulnerability components (e.g. Mueller et al., 2006). However, in recent years, valuable research has been carried out contributing to different vulnerability aspects of geo-risks by the employment of remote sensing-based methods, concepts and data. Vulnerability-related landslide and earthquake applications are in essence very similar as they mainly focus on the same components such as physical building vulnerability, demographic and socioeconomic exposure as well as human and socioeconomic assets. Table 3 sums up pre- and post-event applications and associated sensor groups for both hazard types.

(a) In terms of pre-event risk assessment and management, remote sensing has its main share in the mapping of land cover and land use using multispectral data. For urban areas, this specifically relates to the capturing of elements at risk of the built environment such as buildings and infrastructures. In this context, the potential of remote sensing particularly lies in the generation of spatially accurate building inventories for the detailed analysis of the building stock's physical vulnerability (French & Muthukumar, 2006; Mueller et al., 2006; Taubenböck et al., 2009; Polli & Dell'Acqua, 2011). Vulnerability-related indicators have been derived in various landslide- and earthquake-related studies and include building footprint, height, shape characteristics, roof materials, location, construction age and structure type (Geiß & Taubenböck, 2012). Especially last generation optical sensors featuring very high geometric resolutions (VHR1-2) are perceived as advantageous for operational applications, especially for small to medium scale urban areas in data-poor countries (Deichmann et al., 2011). These data are found to be suitable to quantify and characterize the building stock based on manual image analysis methods, statistical enumeration of samples (Ehrlich et al. 2010) or automatic image information extraction methods (Sahar et al. 2010; Borzi et al. 2011). By the combination of optical sensors with digital elevation information from LIDAR measurements seismic buildings vulnerability can be determined with high accuracies (Borfecchia et al., 2010) whereas the combination of optical and SAR data has proven useful for the retrieval of crucial physical parameters such as building footprint or height (Polli & Dell'Acqua, 2011). Beyond, very high and high (VHR1 to HR1) remote sensing data is suited to characterize homogeneous built-up areas. In this manner, Pittore and Wieland (2012) and Wieland et al. (2012) use this capability in combination with information from a ground-based omnidirectional imaging system to determine the physical vulnerability of the building inventory.

With regard to the analysis of other vulnerability components, remote sensing can deliver further multi-scale geo-spatial information. For the assessment of demo-

graphic vulnerability in particular, several regionalization and disaggregation approaches of census data based on remote sensing products are proposed (e.g, Dobson et al., 2009; Chen, 2002). Furthermore, e.g. Ebert et al. (2009), Taubenböck (2011), and Zeng et al. (2011), use physical proxies retrieved from medium to high resolution (HR1 to MR1) optical and very high resolution (VHR1-2) LIDAR data for the approximation of socioeconomic vulnerability indicators.

(b) **Post-event** vulnerability-related investigations are mainly linked to tasks of damage mapping and assessment as well as the monitoring of the recovery phase and related parameters in the aftermath of an event (Geiß & Taubenböck, 2012). Investigations utilize remote sensing data and techniques for the identification of land cover/land use changes induced by earthquakes or landslides. Similar to pre-event studies, the focus of such applications is on the identification, description and assessment of the present and future conditions of the built and natural environment and hence the elements exposed, however, in the aftermath of an event when structural, demographic and socioeconomic vulnerability is significantly increased.

In this context, remote sensing is a unique tool capable of capturing the up-to-date large-scale damage situation of an affected area (Vu & Ban, 2010). Thus, it has become an operational tool in emergency response, in particular for post-event rapid damage detection, mapping and assessment as well as the provision of crucial information for directing rescue and recovery (Dell'Acqua et al., 2009; Joyce et al., 2009a). Recovery-related parameters in this regard are for example the damage degree of individual and/or significant buildings or entire city blocks or roads and critical infrastructure affected (Kerle, 2010). This information helps emergency organizations in identifying severely impacted-areas and prioritizing response activities as decision support (Eguchi et al., 2003). In this context, post-event rapid damage mapping uses mainly very high and high resolution (VHR1 to HR1) optical and SAR data as the best data source for damage assessment of buildings and infrastructure (Joyce et al., 2009a). However, most operational applications are still limited to manual-visual interpretation techniques to enhance thematic accuracy compared to automated approaches (Trianni & Gamba, 2009). Moreover, even manually derived spatial information products for decision makers often underlie a certain degree of uncertainty due to visual misinterpretation since changes are often only detected for severely damaged structures (Kerle, 2010). Nevertheless, the use of change detection-based methods with multi-date imagery is still perceived to deliver more accurate and reliable results than automated approaches using solely post-event data (Li et al., 2008; Ehrlich, 2008). In this manner, applications are often enhanced by the employment of pre- and post-event LIDAR data to reach a higher level of morphologic detail and accuracy (e.g. Vu et al., 2004; Li et al., 2008). In the case of cloud coverage alternative approaches try to assess the damage situation by the combined use of pre-event optical and post-event SAR data (e.g. Brunner et al., 2011).

In the broader context of post-event event applications, also other elements at risk of the built-environment are under investigation such as critical transportation networks, supply and lifelines by the employment of remote sensing datasets and

products, in particular for the monitoring of post-event recovery and reconstruction activities (e.g. Huang et al., 2009; Wang et al., 2011). Recent applications also try to assess ecologic vulnerability such as the investigation of effects on wildlife habitats (e.g. Xu et al., 2009) or the quantification of damage to the vegetation cover (e.g. Ge et al., 2009) and monitoring of vegetation recovery (Lin et al., 2008) by the use of optical satellite imagery and DEM data.

Tab. 4 Earthquake and landslide vulnerability related remote sensing applications and associated sensor groups / datasets (summarized from van Westen et al., 2008; Joyce et al., 2009a; Geiß & Taubenböck, 2013; bold formatting indicates when a sensor group / associated data set has been identified as being advantageous compared to others mentioned)

<table>
<tr><th colspan="4">Vulnerability-related applications: Earthquake, landslides, etc.</th></tr>
<tr><th>Pre-event application</th><th>Contributing sensor group / associated datasets</th><th>Post-event application</th><th>Contributing sensor group / associated datasets</th></tr>
<tr><td>Mapping of land cover / land use</td><td>Multispectral VHR1-HR1</td><td>Post-disaster rapid and large-scale damage detection, mapping and assessment</td><td rowspan="3">Multispectral VHR1-HR1
DEM / DSM VHR1-2 (LIDAR)
SAR VHR1-HR1</td></tr>
<tr><td rowspan="2">Creation of building inventories and assessment of physiscal vulnerability</td><td rowspan="2">Multispectral VHR1-2
DEM / DSM VHR1-2 (LIDAR)
SAR VHR1-HR1</td><td>Recovery and rescue planing</td></tr>
<tr><td>Reconstruction monitoring</td></tr>
<tr><td>Derivation of physiscal proxies for the assessment of demographic and socioeconomic vulnerability</td><td>Various, specifically:
Multispectral HR1-MR1
DEM / DSM VHR1-2 (LIDAR)</td><td colspan="2"></td></tr>
</table>

GMES (2011): VHR1: <= 1m; VHR2: 1-4m; HR1: 4-10m; HR2: 10-30m; MR1: 30-100; MR2: 100-300; LR: >300m

2. Past- and present-day remote sensing data for vulnerability-related investigations

This chapter identifies several present-day remote sensing systems employed in earthquake and landslide risk analysis. A comprehensive overview of the selected satellite platforms and sensors is given in table 4 including the particular sensor specifications such as geometric resolution, swath width, and revisit capability. A categorization of the spatial scale of analysis is introduced based on the aerial coverage, i.e. the swath-width-dependent scene size, and the geometric resolution of the sensors according. The original scheme was developed by Geiß and Taubenböck (2012) based on the categorization presented by Neer (1999) and harmonized with the data categorization by GMES (2011) for this report. Being aware that, for example, SAR data do not contain the same thematic information as optical data with the same geometric resolution, the categorization is adapted also for non-optical sensors for terms of consistency. The categorization ranges from ‘‘focal’’ to ‘‘local’’ to ‘‘regional’’ to ‘‘national’’ scale of analysis. However, some of the sensors falling under the category “national” also allow ‘‘continental’’ or even ‘‘global’’ analysis.

In general, data with a coarser geometric resolution and larger spatial coverage per scene are able to contribute to overall evaluation in pre- and post-event applications. In contrast, it is yet both difficult and expensive to obtain high geometric resolution data such as airborne LIDAR or VHR optical data over larger areas affected, specifically in case of an earthquake event (Rathje & Adams, 2008). In addition to that, the geometric resolution of the sensors and the associated scene size and thus, the spatial scale of analysis, need always be selected in consideration of the context of the objects to be analysed. For instance, medium resolution remote sensing data can be utilized to accurately analyse large-scale phenomena and objects such as large active faults or mass movements. In contrast to that, vulnerability-related evaluation of small-scale objects such as buildings may, by trend, represent only a rough estimation based on such data.

The following subsections will give an overview and exemplification of present-day remote sensing missions including technical data specifications with regard to each spatial scale of vulnerability analysis.

Tab. 5 Overview of several present-day optical and SAR remote sensing systems employed in earthquake and landslide risk analysis (Source: Categorization of analysis scales from Geiß & Taubenböck, 2012; most sensor characteristics from Joyce at al., 2009a, b, CEOS, 2012 and eoPortal, 2013; Characteristics for "Airborne LIDAR" from Rathje & Adams, 2008, for TanDEM-X from DLR, 2010, for Deimos-1 from ESA, 2012)

Spatial scale of analysis (associated classes of geometric resolution according to GMES, 2011)	Platform/Satellite	Sensor/Mode	Geometric resolution (Nadir) [m]	Swath [km]	Revisit capability	Data availability and data supplier
focal *(VHR1/2)*	**Airborne**	LiDAR	0.5-1	daily coverage of 1-100 km²	Mobilized to order	Usually commercial
	Worldview-1/2	Panchromatic	0.46	16.4	1.1 days	Commercial (Digital Globe)
		Multispectral	1.85			
	GeoEye-1	Panchromatic	0.4	15	<= 3 days	
		Multispectral	1.6			
	Pleiades	Panchromatic	0.5	20	1-2 days	Commercial (Astrium)
		Multispectral	2.8			
	Quickbird	Panchromatic	0.6	16.5	1.5-3 days	Commercial (Digital Globe)
		Multispectral	2.4			
	Ikonos	Panchromatic	1	11	1.5-3 days	
		Multispectral	4			
	Cosmo-Skymed	Spotlight	<1	10	~37 hours	Commercial (e-geos / ASI)
	Formosat-2	Panchromatic	2	24	1 day	Commercial (Astrium)
	TerraSAR-X	Spotlight	1	10	11 day repeat cycle;	Commercial
	TanDEM-L	Stripmap	3	30	2.5 day revisit capability	(Infoterra GmbH)
	EROS A	Panchromatic	1.9	14	10.5 days	Commercial (ImageSat)
	EROS B	Panchromatic	0.7	7	6 days	
	IRS-P5	Panchromatic	2,5	26-30	5 days	Commercial (ISRO)
	IRS-P6	LISS-4	5.8	24	5 days	
	ALOS	PRISM	2.5	70	Several times per year as per JAXA acquisition plan	Commercial (JAXA)
	Radarsat-2	Ultra-fine	3	20	Every few days	Commercial (CSA)
local *(HR1)*	**SPOT-1/2/3**	PAN	10	117	1-4 days	Commercial (Astrium)
	SPOT-4/5	Panchromatic	5	60-80	11 times every 26 days	
		Multispectral	10	60-80		
	Formosat-2	Multispectral	8	24	1 day	Commercial (Astrium)
	Rapid Eye	Multispectral	6.5	77 x 1500	1 day	Commercial (RapidEye AG)
	ALOS	AVNIR	10	70	Several times per year as per JAXA acquisition plan	Commercial (JAXA)
		PALSAR (Fine)	7-44	40-70		
	Radarsat-1/-2	Fine	8	50	Every few days	Commercial (CSA)
regional *(HR2/MR1)*	**Landsat-1/2/3**	Multispectral (MSS)	20/80	117/185	Every 18 days	Free (USGS)
	Landsat-4/5	Multispectral (TM)	30	185	Every 16 days	
	Landsat-7	Panchromatic (ETM+)	15	185		
		Multispectral (ETM+)	30			
	Landsat-8	Panchromatic (OLI)	15	185	Every 16 days	
		Multispectral (OLI)	30			
	SPOT-1/2/3	Multispectral	20	117/185	1-4 days	Commercial (Astrium)
	TerraSAR-X TanDEM-L	ScanSAR	18	100	11 day repeat cycle; 2.5 day revisit capability	Commercial (Infoterra GmbH)
	Radarsat-1/-2	fine	25	100	Every few days	Commercial (CSA)
		Wide	30	150		
	ERS-2		30	100	35-day repeat cycle	Commercial (ESA)
	Deimos-1	Multispectral	22	600	1 day	Commercial (Astrium)
	Terra	ASTER - VNIR	15	60	Every 16 days	Partly free (NASA)
		ASTER - SWIR	30	60		
		ASTER - TIR	90	60		
	SRTM	X-Band	30	220	-	Free (USGS)
	Envisat	ASAR standard	30	100	36 days	Free (ESA)
	IRS-P6	LISS-3	23.5	141	5 days	Commercial (ISRO)
national *(MR2/LR)*	**ALOS**	PALSAR (ScanSAR)	100	250-350	Several times per year as per JAXA acquisition plan	Commercial (JAXA)
	Landsat-5	TM Thermal	120	185	Every 16 days	Free (USGS)
	Lansat-7*	ETM+ Thermal	120	185	Every 16 days	Free (USGS)
	Radarsat-1/-2	ScanSAR wide	100	500	Every few days	Commercial (CSA)
	Terra /Acqua	MODIS	250, 500, 1000	2300	At least twice daily for each satellite	Free (USGS)
	NOAA	AVHRR	1100	2399	Several times per day	Free (USGS)
	DMSP	OLS fine	560	3000	~ 12 hours	Free (NOAA)
		OLS smoothed	2700	3000		
	Envisat	MERIS	300	575	36-day repeat cycle	Free (ESA)
		ASAR ScanSAR	1000	405	36-day repeat cycle	

GMES (2011): VHR1: <= 1m; VHR2: 1-4m; HR1: 4-10m; HR2: 10-30m; MR1: 30-100; MR2: 100-300; LR: >300m

2.1 Focal and local scale

On the focal and local scale of analysis very high and resolution (VHR1 to HR1) optical, LIDAR and SAR data are used to map, assess, and monitor land cover, land use and especially the physical/structural face of the built environment such as buildings, infrastructure and lifelines, which represent critical components of risk management and loss estimation methodologies (Tralli et al., 2005).

In this context, the integration of optical satellite remote sensing data with digital elevation information derived from D-InSAR measurements or airborne laserscanning has been studied intensively in vulnerability-related investigations of urban areas (e.g. Gamba & Houshmand, 2002; Borfecchia et al., 2010; Polli and Dell'Acqua, 2011, etc.). Featuring geometric resolutions ranging from 4 to <1m, these datasets provide the ability to cover the small scale and heterogeneous urban morphology for vulnerability assessment and rapid post-disaster damage detection (Rejaie and Shinozuka, 2004). Furthermore, the relatively short revisit capabilities of up to 3 days allow for the utilization in multi-temporal applications such as pre- to post-event change detection. Through integration with demographic data, infrastructure and building stock databases using methodologies of geographic information science such as regionalization techniques and dasymetric mapping these data can be further used to approximate demographic and socioeconomic variables by physical proxies. Thus, available satellite remote sensing systems, from civil space agencies and commercial imaging sources are witnessing increased utilization in disaster management research and operational domains.

A very high resolution optical sensor (VHR1-2) commonly applied in vulnerability-related applications on the focal scale is Ikonos. Ikonos data feature a geometric resolution of one meter panchromatic, four meter multispectral and one meter pan-sharpened. The high-end geometric capability of Ikonos enables the derivation of highly detailed urban structures. Apart from these data, many sensors such as Quickbird, Worldview and GeoEye with similar technical details allow for comparable analysis. On the local scale, the German RapidEye constellation of five satellites launched in 2008 features a revisit time of one day with a slightly coarser spatial resolution of 6.5m. Overall, the high spatial and temporal resolution of these sensors holds great potential for pre- and post-event vulnerability monitoring.

Radar remote sensing has the distinct advantage of acquiring imagery independent from weather and time of day. The German satellite TerraSAR-X (TSX) launched in June 2007 is one prominent example. Featuring a geometric resolution of up to 1m in Spotlight mode and 3m in Stripmap mode it is regarded as another useful option for disaster monitoring. Its partner satellite TanDEM-X (TDX) was launched in 2009 in a close orbit, allowing for the generation of high resolution (HR1) DEMs of 12m spatial resolution by interferometric imaging techniques that could potentially be used for change analysis, particularly with respect to volumetric analysis of landslide-related earth movement (Joyce et al., 2009a). Further SAR systems suitable for analysis on

the focal and local scale featuring similar spatial and revisit capabilities are Radarsat 1 / 2, Cosmo Skymed, etc. (Geiß & Taubenböck, 2012).

2.2 Regional scale

On a regional scale of analysis, the applicability of remote sensing datasets and methods is limited, mainly due to the affiliated geometric resolution (HR2 to MR1) and revisit capabilities of the particular sensor. However, due to relatively large swath width and the multispectral information contained, especially optical remote sensing data are widely employed for large-scale mapping of the exposed land cover and use. In conjunction with location and extent of hazards such as landslides or floods derived from multispectral or SAR data using manual and automated techniques (Joyce et al., 2009a), these data can contribute to the post-event large-scale damage assessment in terms of a rough estimate of the affected land use (e.g. Aydöner & Maktav, 2009; Chang & Tang, 2010; Taubenböck et al., 2011). In this manner, various sensors are suitable for the generation of large-scale and accurate land use databases. Based on these data, several authors have further tried to derive indicators of regional demographic vulnerability such as regional population inventories (e.g. Aubrecht et al., 2012) or social vulnerability on county level (e.g. Zeng et al., 2011) by the application of regionalization techniques. Furthermore, medium resolution (MR1) DEM data derived from the Shuttle Radar Topography Mission (SRTM) is commonly used for the coarse localization of hazard-prone regions, e.g. by the assessment of terrain elevation in case of tsunami flooding or the computation of aerial slope steepness in case of landslide events (e.g. Taubenböck et al., 2008). Relating to vulnerability-centred applications, medium resolution (MR1) EO data is also frequently used for the regional assessment of hazard-affected areas, above all for the determination of location and extent of hazards in the post-disaster phase.

The Landsat series of sensors (Multispectral Scanner (MSS), Thematic Mapper (TM), Enhanced Thematic Mapper (ETM+)) provide large-scale observations covering spatial extents of up to 185km for large-scale conurbations such as megacities, as well as data continuity due to repetitive and continuous monitoring. Accordingly, the eights and latest satellite from the Landsat series was launched on February 11, 2013. It carries the Operational Land Imager (OLI) and the Thermal Infrared Sensor (TIRS). OLI collects data from nine spectral bands, which cover the range from visible to short wavelength infrared. The bands feature a geometric resolution of 30m, whereas the panchromatic band allows a geometric resolution of 15m. The TIRS instrument collects data in two long wavelength bands with a geometric resolution of 100m to allow for thermal imaging (USGS, 2013). The sun-synchronously orbiting Landsat sensors are a cost-effective choice as imagery is provided free of charge by the United States Geological Survey (USGS). A further distinct advantage is data comparability due to the arrangement of spectral bands within the same spectral regions. However, the sensors' relatively coarse geometric resolution presents one weakness with regard to classification due to subpixel mixed spectral information. Nevertheless, the particular datasets allow for the accurate land cover classification, especially of the distribution of urban areas in their correct dimension and form (Taubenböck et al., 2012a) as a first indicator

of the spatial arrangement of human and structural exposure. Furthermore, multi-temporal imagery allows for the rough estimation of building ages and spatial urbanization rates by post-classification comparison as important vulnerability inidicators. In addition, homogeneous urban structure types can be discriminated and characterized based on such data (Wieland et al., 2012).

The new German radar missions of TSX and TDX have acquired two coverages of the entire landmass of the world for 2011 and 2012 which is utilized for the classification of a global urban footprint (Taubenböck et al., 2012b). Further optical and active radar sensors applied in the regional land cover mapping context are Radarsat-1/2, ERS-2, ASTER and Envisat. DEM data often utilized for hazard- and vulnerability-related investigations stems from the SRTM. This interferometric DEM is based on X- and C-Band data and commonly used to assess terrain situation, especially with regard to flood to landslide hazards (e.g. Taubenböck et al., 2008 & 2011; van Westen et al., 2008). With a pixel spacing of 1 x 1 arc seconds to a maximum of 3 x 3 arc seconds (~ 25-90m) and a vertical accuracy of < 20m it enables a rather coarse overview of the earth surface. In this context, TDX and TDX will provide a more detailed surface representation with global coverage of 12m grid spacing in the near future (Huber et al., 2010).

2.3 National scale

Remote sensing applications that use very low to medium (MR2 to LR) resolution data on the national scale of analysis are limited to the mapping of large-scale human and physical exposure. In this context, various multi-scale geospatial information products and approaches to model and assess situation-specific earthquake-related population exposure are presented by Aubrecht et al. (2012). Remote sensing derived land cover maps are used as a basis for the disaggregation process (Eicher & Brower, 2001; Mennis & Hultgren, 20006; Langfrod, 2007) and geo-products ranging from national to global coverage have been derived. These are frequently used as a first approximation of exposed assets in the context of sampling approaches.

The MODIS sensors on-board the NASA satellites Terra and Acqua acquire surface data from the visible to the near-infrared through mid-infrared wavelengths (with 36 spectral bands) with a swath width of 2300 km. Although the spatial resolution of MODIS data only ranges from 250m (2 visible bands), to 500m (5 visible to shortwave infrared bands), and to 1000m (29 visible, near infrared, shortwave infrared, and mid-infrared bands) (Parkinson & Greenstone, 2000), the sensor allows monitoring the often large-scale land use phenomena. In this context, a thematically detailed land cover type data set has been derived from the sensor’s data. The MODIS Land Cover Type product contains five classification schemes, which describe land cover properties derived from observations spanning a year’s input of Terra- and Aqua-MODIS data.

The Operational Linescan System (OLS) on-board the Defence Meteorological Satellite Program’s (DMSP) Satellite F13 measures visible (0.4-1.1 micrometers) and infrared (10.25-12.6 micrometers) wavelengths. The satellite measures data at a 0.56km reso-

lution, which is filtered and averaged on board to efficiently store imagery of global coverage at 2.7km resolution. Being very sensitive in the visible wavelength region, OLS can detect even very faint light from the earth's surface at night which is archived since 1992. Due to the spatial correlation of urban settlements and night time lights several studies have aimed at mapping urban exposures using OLS data (e.g. Imhoff et al., 1997; Small et al., 2005).

Further acquisition systems with similar technical specifications are ALOS, Radarsat's ScanSAR wide acquisition mode, NOAA A VHRR, and Envisat. A comprehensive overview of remote sensing derived geo-products for exposure mapping is presented in chapter 4.

3. Future remote sensing missions

From a technical point of view, the constantly increasing availability and accessibility of remote sensing imagery provides new opportunities for a wide range of applications of geo-risk research. One of the main limitations to applications, however, still is data costs. While satellite data for regional or national scales are in general moderately priced or even free of charge, detailed analysis on local and focal scales often require three-dimensional surface representations, where mostly airborne or high to very high (VHR1-2) resolution optical satellite data and thus cost-intensive remote sensing data is required. For area-wide coverage of large-scale test sites with VHR images, e.g. entire cities or even mega cities, these are often too high and beyond the financial resources of local authorities. In this context, sampling approaches, which use medium resolution image analysis to select areas to be analysed in greater detail with VHR imagery or ground-based survey techniques, become more applicable (Wieland et al. 2012). Therefore, future spaceborne missions such as the Sentinel programme of the European Space Agency (ESA, 2013) aim at securing data continuity and free-of-charge availability of medium and high resolution (MR1 to HR1) ERS, Envisat and SPOT-like observations (Berger & Aschbacher, 2012) to service providers and the scientific community since the technical lifetime of past missions such as Landsat-4/5 and Radarsat-1 (both by 2012) as well as SPOT-4, IRS-P5, TSX and Terra (all by 2013) (eoPortal, 2013) will come to an end.

A selection of promising launched, planned or proposed missions are presented in this chapter. A comprehensive overview of the selected satellite platforms and sensors is given in table 4 including the particular sensor specifications such as geometric resolution, swath width, and revisit capability – if specified yet. Again, a categorization regarding the spatial scale of analysis is applied based on the aerial coverage, i.e. the swath-width-dependent scene size, and the geometric resolution of the sensors according to the harmonized classification scheme presented by GMES (2011).

The sensors listed include *ALOS-2* (L-band SAR system with a geometric resolution of 1–10 m; JAXA 2011), the *RADARSAT constellation* (planned as a high resolution C-band mission of three to six satellites it includes high-resolution modes at 3 and 5 m, which were primarily designed for disaster management; CSA, 2012), *DESDynI* (L-band SAR with a geometric resolution of 10m and a multiple beam LiDAR instrument with a geometric resolution of 25m and 1m vertical accuracy; DESDynI, 2011), *CARTOSAT-3* (multispectral sensor with a geometric resolution of 0.25m panchromatic; Katti et al. 2007), *ALOS-3* (optical sensor with a geometric resolution of 0.8m panchromatic and the capability to acquire stereo images with a swath of 50 km; eoPortal, 2013), the Sentinel mission sensors (optical and C-band SAR sensors that will provide free datasets of down to 10m and 5 m, respectively, ESA, 2013), *TerraSAR-X 2* (featuring an advanced SAR sensor technology allowing a spatial resolution down to 0.25m), *TanDEM-L* (enabling systematic, area-wide and high resolution interferometric monitoring, Moreira et al., 2011), *WorldView-3* (superspectral sensor with a geometric resolution of 0.31m panchromatic; DigitalGlobe, 2012) or *EnMAP* and *HyspIRI* (hyperspectral

sensors with a geometric resolution of 30m and 60 m, respectively; Heldens et al. 2011) have the potential to play a key role in future earthquake and landslide investigations. Thereby, the tasking of satellites (constellations) becomes more important in order to be able to provide the right images at the right time with the appropriate characteristics. In general, future missions will continue the path of current missions or even enlarge the capability for hazard-, exposure-, vulnerability-, damage- and recovery-related remote sensing to develop and provide relevant geoinformation products for monitoring.

In conclusion, to assess data and service continuity of past-, present- and future day remote sensing mission a comprehensive overview of satellite lifetimes is given in table 7.

Tab. 6 Overview of several future remote sensing missions that could be employed in earthquake and landslide risk analysis (Source of sensor specifications: ALOS-2 (JAXA, 2011), ALOS-3 (eoPortal,2013), Cartosat-3 (Katti et al., 2007), TerraSAR-X 2 (Janoth et al., 2012), Radarsat Constellation (CSA, 2012), TanDEM-L (Moreira et al., 2011), WorldView-3 (Digital Globe, 2012), Sentinel-1/2 (ESA, 2013), DESDynI (DESDynI, 2011), EnMAP & HySPIRI (Heldens et al., 2011), SPOT-6/7 (eoPortal, 2013))

Spatial scale of analysis (associated classes of geometric resolution according to GMES, 2011)	Platform/Satellite	Planned Launch	Sensor/Mode	Geometric resolution (Nadir) [m]	Swath [km]	Revisit capability
focal *(VHR1/2)*	**ALOS-2**	2013	Spotlight	1-3	25	14 days
	ALOS-3	2013	Multispectral Scanner with high stereo acquisiton capability	0.8	50	14 days
	Cartosat-3	2015	PAN VIS	0.25	15	one week min. (tbs)
	SPOT-6/7	2012/2014	Panchromatic	1.5	60	1 day
	TerraSAR-X 2	2016	Spotlight	0.25/0.5/1	5/10/15	11 days
			Strip Map	3	24	
	Radarsat Constellation	2018	C-Band Very high resolution	3	20	4 days
	TanDEM-L	2019	L-Band SAR	tbs	350 (tbs)	8 days
	WorldView-3	2014	PAN VIS	0.3	13.1	< 1 day
			Multispectral	1.24		
			SWIR	3.7		
local *(HR1)*	**Sentinel-1**	2013	Wave	5	20	12 days (one satellite)/6 days (two satellites)
	SPOT-6/7	2012/2014	Multispectral	8	60	1 day
	Sentinel-2	2014	VIS	10	290	10 days (one satellite)/5 days (two satellites)
	ALOS-2	2013	Strip Map	3-10	50/70	14 days
	TerraSAR-X 2	2016	TOPS	5/12	50/100	11 days
	Radarsat Constellation	2018	C-Band High Resolution	5	30	4 days
	DESDynI	2021	L-Band InSAR	10	tbs	tbs
regional *(HR2/MR1)*	**Sentinel-1**	2013	Interferometric Wide Swath	5 x 20	250	12 days (one satellite)/6 days (two satellites)
	Sentinel-2	2014	NIR	20	290	10 days (one satellite)/5 days (two satellites)
			SWIR	60		
	TerraSAR-X 2	2016	TOPS	30	400	11 days
	Radarsat Constellation	2018	C-Band Medium Resolution	16/30/50	30/125/350	4 days
	EnMAP	2015	Hyperspectral	30	30	23 days (Quasi Nadir 0-5°) 4 days (Off-Nadir 0-30°)
	HyspIRI	2020	Hyperspectral	60	145	5 days (TIR), 19 days (SWIR)
	DESDynI	2021	Multiple beam LIDAR	25	tbs	tbs
national *(MR2/LR)*	**ALOS-2**	2014	Scan SAR	100	350/490	14 days
	Radarsat Constellation	2018	Low Resolution	100	500	Daily

GMES (2011): VHR1: <= 1m; VHR2: 1-4m; HR1: 4-10m; HR2: 10-30m; MR1: 30-100; MR2: 100-300; LR: >300m
tbs = to be specified

3.1 Sentinel Mission

Five new missions, called Sentinels, are currently being developed by the European Space Agency (ESA). The first satellite of the Sentinel series is planned to be launched in 2013. Overall, the satellites are specifically designed to adapt to the operational needs of the GMES programme. Carrying a wide array of sensor systems such as radar and multi-spectral imaging instruments, the satellites will provide large-scale observations and capabilities in terms of repetitive and continuous monitoring (ESA, 2013). The first two missions, Sentinel-1 and –2, are planned to be launched in 2013 and 2014, respectively.

The Sentinel-1 satellite system is designed to enable continuation of C-band SAR operational applications following Europe's and Canada's series of SAR systems such as ERS-1, ERS-2, Envisat and Radarsat. With regard to GMES user services and requirements the application focus is mainly on (1) monitoring of sea ice zones and the arctic environment, (2) surveillance of marine environments, (3) monitoring of land surface motion risks, (4) mapping of land surfaces, and (5) mapping in support of humanitarian aid in crisis situation (ESA, 2013). Carrying a C-band imaging radar system, Sentinel-1 is capable of acquiring data independent from weather and time of day at global coverage. Featuring two main operational modes, images will be acquired with a 5 x 20m ground resolution and a 250km swath width in interferometric wide swath mode and at 5m ground resolution and a 20km swath in wave mode (Torres et al., 2012). Sentinel-1's revisit capabilities, spatial coverage and fast-track data dissemination are key features of the mission requirements in the framework of GMES. As a big enhancement compared to existing SAR systems, data will be disseminated within an hour of acquisition. The capabilities of the new system for the monitoring of land-surface motion risks are widely recognized. For example, Salvi et al. (2012) emphasize that the Sentinel-1 program will allow for an effective coverage for interferometric data over earthquake-prone regions at global level. With a revisit cycle of 12 days with one satellite, and 6 days with both, these data are considered to have the potential to substantially improve scientific knowledge and allow geodetic operational monitoring of the seismic changes. With respect to the on-going TSX and TDX missions and the related "Global Urban Footprint" initiative of DLR (Esch et al., 2012) this ESA mission holds high capabilities for continuative exposure mapping or continuative urban monitoring. Taubenböck et al. (2012) already successfully transferred and tested the originally developed classification algorithm for built-up area detection using the X-band data of TSX to the C-band of Canadian Radarsat-2 data. The transfer of the approach shows a robust classification with high overall accuracies exceeding 90%.

Fig. 2 Artist impression of Sentinel-1 satellite (Torres et al., 2012)

The Sentinel-2 series of satellite are designed to deliver high to medium resolution (HR1 to MR1) optical imagery at global coverage in continuation of previous optical missions such as Landsat and Spot (Berger & Aschbacher, 2012) but with enhanced geometric and spectral capabilities. The first satellite is planned to be launched in 2014. With regard to the payload specifications, the platform will carry sensors sensitive in the visible (4 bands at 10m resolution), near infrared (6 bands at 20m resolution) and shortwave infrared (3 band at 60m resolution) wavelength regions capturing imagery at a swath width of 290km. Similar to the Landsat series of sensors that enabled multi-temporal acquisition since the early 1970s, the superspectral system will enable consistent multi-temporal image acquisition. Orbiting at an altitude of roughly 800km the pair of satellites has a revisit time of five days at the equator and two to three days in mid-latitudes.

The higher spatial resolution in combination with a higher spectral resolution and a large swath enables to cover large urban areas such as mega cities at once. Thus, Sentinel-2 will provide immense potential for exposure-related remote sensing by means of land cover classification as the acquired data allow both for the enhancement of the geometric precision of e.g. urban footprint products as well as an increased depth of thematic class detail by their superspectral capabilities. These improvements may allow refining the urbanized areas into structural types, such as classes based on built-up density or even to aim at classifying semantic structural types such as slum areas, central business districts or industrial sites. Thus, monitoring is not only to be continued but to be thematically more detailed using the future Sentinel-2 mission. Furthermore, images of hazard events such as landslides, volcanic eruptions, and floods will be acquired to determine hazard location and spatial extent. The capability of delivering time-critical data is ensured by a very shot repeat cycle of the two-satellite-constellation. Thus, Sentinel-2 imagery will provide a reliable data basis both for thematically detailed land-cover classifications and the derivation of frequent land-

change detection products. In essence, Sentinel-2 combines a large swath, frequent revisit, and systematic acquisition of all land surfaces at high-spatial resolution and with a large number of spectral bands, surpassing the overall capabilities of past missions (ESA, 2013).

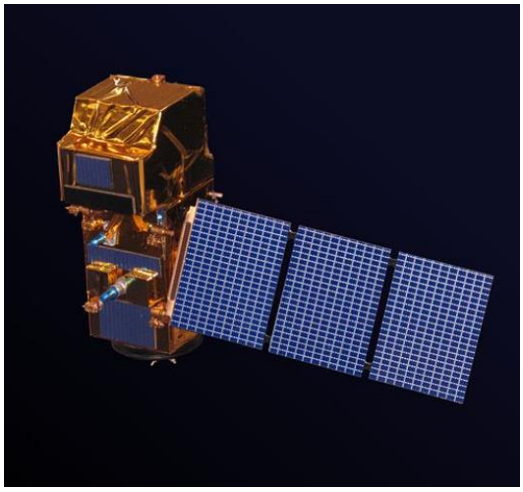

Fig. 3 Sentinel-2 satellite (ESA, 2013)

3.2 ALOS Mission

The Advanced Land Observing Satellite-2 (ALOS-2) also nicknamed „DAICHI-2“ is a planned JAXA follow-up mission. Since 2006, the first satellite ALOS (“DAICHI”), has delivered valuable data for cartographic monitoring on a regional scale, as well as disaster monitoring and resource surveys acquiring data using L-band SAR technologies. ALOS-2 will succeed this mission with enhanced capabilities enabling analysis on the local and even focal scale. Again, carrying a state-of-the-art L-band SAR system, ALOS-2 scans the earth’s surface at Spotlight mode (1-3m ground resolution and 25km swath width) and Stripmap mode (3-10m ground resolution and 50 to 70km swath width) enabling a geometrically more detailed monitoring of disasters than its predecessor. The enhanced instrument performance of ALOS-2, enabled through the right-and-left looking observation capability, will greatly expand the field of regard (FOR; the area covered for the detector of the system when pointing to all mechanically possible directions) of the satellite, up to about 3 times (from 870km on Daichi to 2,320 km) for hazard monitoring services. JAXA is currently investigating applications employing ALOS-2’s observational capabilities such as landslide and earthquake disaster monitoring and damage assessment of hazard-affected areas (JAXA, 2012).

The capability of providing a high geometric resolution with a large up 50km broad swath will significantly improve the coverage for these kinds of data. Especially in the urban domain, where a 50km swath often covers entire cities, area-wide city classification will be possible instead of limitations to quarters due to data costs. For example, very high resolution (VHR1) optical sensors such as Ikonos or Quickbird only

have swath widths of 10 to 15km. Thus, it becomes obvious which capabilities the ALOS-2 sensor holds for urban applications. Applications for entire cities such as on urban structure types (Wurm et al., 2009), energy-relevant questions (Geiß et al., 2011), risk and vulnerability (Taubenböck et al., 2008), amongst many others are typical fields.

Fig. 4 Artist impression of ALOS-2 satellite (JAXA, 2012)

Similar to ALOS-2, ALOS-3 is a follow-up on previous JAXA missions in the optical domain complementing SAR services of ALOS-2. ALOS-3 features two optical sensors. A multispectral Scanner called PRISM-2 with very high resolution (VHR1) stereo acquisition capability and high geo-location accuracy acquires imagery at sub-meter spatial resolution and a swath width of 50km allowing for the generation of highly detailed DSMs by the employment of stereo imaging techniques. ALOS-3 will also deliver very high resolution pan-sharpened images with simultaneous acquisition of images (both nadir- and backward-looking) and four-band multi-spectral images. Two important targets of the ALOS-3 mission in the geo-risk context are monitoring and damage assessment of hazard-affected regions and continuous updating of the national geographical data inventories, including topographic information, land use, and vegetation cover (eoPortal, 2013).

With regard to the RADARSAT Constellation and TerrSAR-X2 missions (see below), the ALOS-3 mission will add to the general area-wide data availability. From a multi-source point of view, users will gain a large data basis of consistent and frequently updated coverage with comparable data sets. Thus, the EO-capabilitiy, especially when applications are time-relevant such as natural hazards affecting urban areas, will increase significantly.

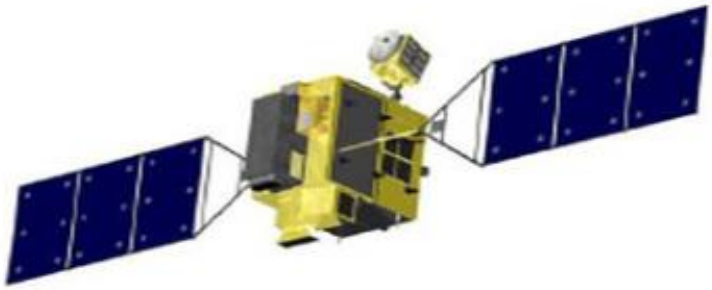

Fig. 5 ALOS-3 satellite (eoPortal, 2013)

3.3 WorldView-3

With WorldView-3, the commercial image supplier Digital Globe will launch the first super-spectral, very high-resolution (VHR1) optical sensor system in 2014. Operating at a polar orbit of 617km height, WorldView-3 will deliver panchromatic imagery at 31cm geometric resolution in addition to 1.24m multispectral and 3.7m shortwave infrared imagery. With its daily revisit capability, the sensor will gather ground information of 680,000km² per day (Digital Globe, 2012). Beyond that the sensor will provide stereo image pairs of 27km width allowing for the generation of VHR digital surface models.

Thus, the availability of digital height information at highest resolution will significantly increase in the near future, which is a central prospect in complex exposed urban morphology. To date remote sensing is often restricted with regard to area-wide coverage of entire cities with 3-D building inventories owing to data costs or other availability restrictions. This could be partially solved due to the large area-coverage of future missions. This means that VHR optical (as well as stereo) data sets will by broadly available and research questions will more and more disengage from problems of VHR data availability and shift to investigations of relevant information derivation, such as highly detailed urban feature extraction, structural vulnerability estimation as well as rapid post-event damage detection.

3.4 Cartosat-3

Cartosat-3 will be the fifth satellite of the Cartosat series scheduled by the Indian Space Research Organisation (ISRO) for 2015. The platform-carried sensor will feature a 0.25m ground resolution and a 15km swath with stereo imaging capability for the generation of very high resolution (VHR1) digital surface models (Katti et al., 2007). Potential uses include weather mapping, basic cartographic and strategic applications but also the derivation of detailed building inventories for physical vulnerability assessments of urban areas.

Stereo mapping is a high importance for mapping exposure as elements at risk do not only feature a 2-dimensional layout but also a 3-dimensional one. From the combination of optical VHR data and a digital surface model, a 3-dimensional city

model allows the analysis of urban morphologies in much higher detail. Similar to WorldView-3, Cartosat-3 will add to the capabilities of remote sensing add to the increase of VHR data availability and applications of urban feature extraction.

3.5 TerraSAR-X 2

The TerraSAR-X 2 mission is to continue TSX services and to provide very high to high (VHR1 to HR2) resolution X-band SAR imagery with improved performance parameters to the user community from 2016 onwards. The mission will feature an enhanced SAR technology enabling very high ground resolutions of down to 0.25m in Spotlight mode (5 to 15km swath width) and 3m in Stripmap mode (24km swath width). Beyond this, TSX 2 will feature two terrain observation by progressive scan (TOPS) modes at 5 and 12m (50 and 100km swath width, respectively) as well as 30m (400km swath) at a repetition rate of 12 days to ensure TerrSAR-X data continuity for large-area applications. The Mission will be arranged in a partnership model called “WorldSAR” through which partners can participate and subscribe on a commercial basis (Janoth et al., 2012).

With these specifications, TSX 2 will provide valuable geo-information for hazard- as well as vulnerability-related applications on various spatial scales of analysis. Beyond that, the continuation of the TSX as well as TDX missions would allow for a systematic continuation of large area coverage for urban monitoring. As these systems are already well suited for the derivation of a new global urban layer (described below), this new mission featuring a significantly improved spatial resolution is predestined to continue this process. Beyond the binary classification of urbanized and non-urbanized areas, these data even hold the potential to derive information on building density and building volume.

Fig. 6 Artist view of TSX satellite (Janoth et al., 2012)

3.6 TanDEM-L

The TanDEM-L (TDL) mission proposed for the year 2019 aims at a systematic, large-scale polarimetric and interferometric monitoring of global coverage (Moreira et al., 2011) that should enable analysis of dynamic earth processes such as – among many others - ground displacements in the range of milimeters or 3-dimensional structure changes of the earth's surface by advanced SAR imaging techniques (Krieger et al., 2009). Although not fully specified yet, sensor specifications will include a very high resolution L-band SAR acquisition system of wide swath (around 350km) and short revisit cycles. The mission will open up opportunities to better understand the earth's dynamic surface processes such as correlations between tectonic displacements and strain build-up or relaxation (Eineder et al. 2009; Minet et al. 2008) may assist in better understanding the physics of earthquakes. The motivation of this mission is based on the increasing scientific requirements for continuous global monitoring of climate and environmental variables with very high geometric resolution. Thus, specific applications relating to earthquake hazard analysis further include earth surface deformation monitoring e.g. due to seismic ground motion, volcanic activities, landslides, soil subsidence or uplift as well as the monitoring of hazard-related parameters such as changes of surface soil moisture, vegetation cover and land use specifically with regard to landslides.

3.7 Radarsat Constellation

RADARSAT Constellation is the continuation of the Canadian Space Agency's SAR satellite program with the objectives of ensuring C-band data continuity and improving the operational use of SAR data. The core user focus of the constellation will be on disaster management, maritime surveillance and ecosystem monitoring. The three-satellite constellation is planned to be launched in 2018 with mission development having begun in 2005. The current baseline configuration foresees three platforms but is extendable to a further three satellites. The sensor system covers the range from low resolution (MR2 at 100m) to medium and high resolution acquisition modes (HR2 to MR1 at 16/30/50m) to high (HR1 at 5m) and very high (VHR2 at 3m) resolution imagery primarily designed for disaster management.

This configuration enables both monitoring of spatially extensive geographic areas as well as small-scale landscapes with varying swath widths (CSA, 2012). An enhanced temporal revisit capability of four days will foster advanced interferometric applications enabling the generation of very accurate coherent change maps for the assessment of earthquake or landslide-induced surface changes and damage detection. With regard to exposure-related mapping, Taubenböck et al. (2012) already successfully tested an algorithm originally developed using the X-band data of TSX for classification of urbanized areas to the C-band of Canadian Radarsat-2 data. The transfer of the approach shows a robust classification with high accuracies. Thus, this mission ensures large-scale, up-to-date spatial data for continuation of consistent monitoring of urban areas and their temporal evolution over time.

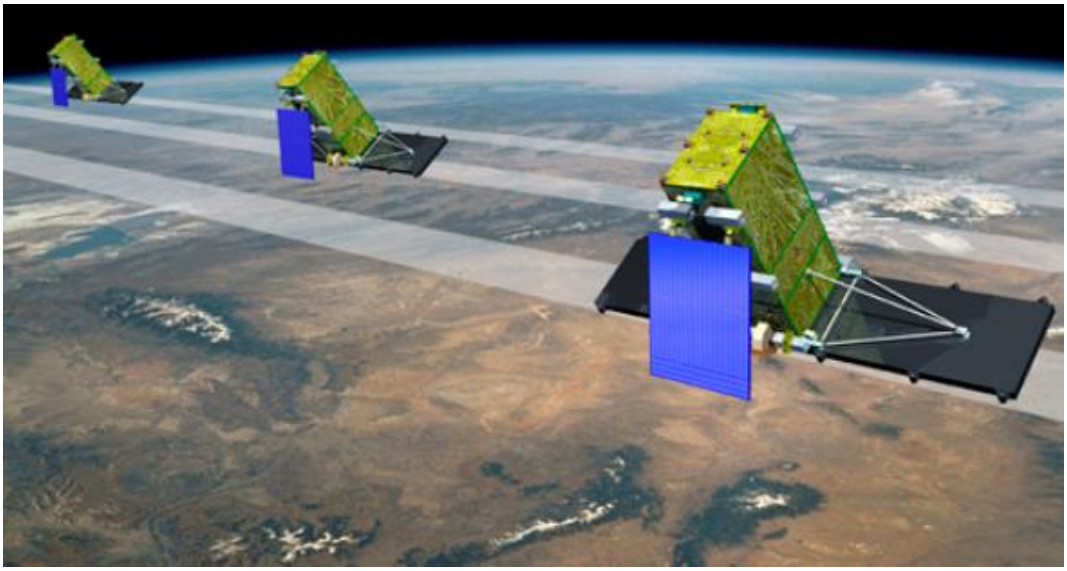

Fig. 7 Artist view of Radarsat Constellation satellites (CSA, 2012)

3.8 DESDynI

This NASA “Deformation, Ecosystem Structure and Dynamics of Ice” (DESDynI) mission is scheduled for 2021 and planned to combine two sensor systems which will enable – in combination – observations critical for the earth surface deformation monitoring. These sensors are a multiple-polarization L-band Interferometric Synthetic Aperture Radar (InSAR) system and a multiple-beam infrared LIDAR system capturing data at 10m and 25m spatial resolution, respectively. The mission requirements are determined to meet the geodetic measurement precision of interferometric SAR technologies for the accurate monitoring of surface deformations and thus, the predictive determination of earthquake and landslide likelihoods. Orbiting sun-synchronously at 700-800km height with an eight day repeat cycle balances temporal de-correlation with required coverage. The mission is planned for a 5 year period to temporally cover time-variable processes and achieve measurement accuracy.

3.9 EnMAP / HySpIRI

Hyperspectral monitoring enables to accurately study the condition of Earth's surface and the changes affecting its ecosystems. In the context of natural hazard risks, hyperspectral data are further frequently employed for the estimation of physical vulnerability parameters in urban areas (Heldens et al., 2012), land cover-based exposure mapping or – on the local scale – detection of rock failures with regard to landslides (Joyce et al., 2009a). With the German program “Environmental Mapping and Analysis” (EnMAP) a new state-of-the-art Hyperspectral Imager (HSI) is planned to be launched in 2015. EnMAP will monitor the Earth's surface at a geometric resolution of 30m and a 30km swath. Spectral bands will continuously cover the 420-2450nm

wavelength range by means of two spectrometers covering the visible to near-infrared (VNIR) and the short-wave infrared (SWIR) spectral regions over 244 bands. Due to an off-nadir pointing device with an adjustable angle of up to 30° the sensor features a minimum revisit time of 4 days (GFZ, 2012). A similar sensor is NASA's Hyperspectral Infrared Imager (HyspIRI) featuring wavelength coverage in the visible, shortwave infrared, mid and thermal infrared regions in contiguous bands of 10nm spacing (NASA, 2013). However, with a minimum revisit capability of 5 days and a coarser spatial resolution of 60m at nadir the technical capabilities are surpassed by EnMAP.

The expected high data quality of the EnMAP sensor and its extensive spatial coverage of 900km² per scene open up new possibilities for the upscaling of existing imaging airborne spectroscopy approaches with limited spatial coverage. However, a direct transfer of these methods to spaceborne imaging spectroscopy will be challenging because of the difference in spatial resolution between airborne and EnMAP HSI data (Heldens et al., 2012). Nevertheless, following up the expected enhanced capabilities of Sentinel-2, the hyperspectral capabilities of EnMAP with a spatial resolution of 30m will allow information extraction with thematic details beyond that. Heldens et al. (2011) reviewed 146 publications to give an outlook on the capabilities of the sensor. They mention four application fields regarding the urban domain: (1) urban development and planning applications might be improved by enhanced capabilities of mapping built-up areas by impervious surfaces (i.e. surfaces impenetrable by water as such as sidewalks, driveways, rooftops and parking lots as indicator for urban functional land use), vegetation fractions, materials, urban structure types and biotopes. Regarding, (2) urban growth assessment by change detection will be enhanced by the capabilities for consistent monitoring of building and respective material changes, (3) risk and vulnerability assessment and especially could be thematically enhanced by hazardous materials detection (4) urban climate applications will be improved due to better mapping capabilities of material-based land cover and building and vegetation structures.

The Hyperspectral Infrared Imager of the HyspIRI mission with the thematic focus of studying the world's ecosystems and the provision of critical information on natural disasters such as volcanoes, wildfires and droughts is not expected to be capable of to maintaining or further improving the thematic depth of urban mapping compared to EnMAP. However, this mission with a 600km swath might enable large-scale monitoring of urban areas and is thus, especially when thinking continental or global, an interesting sensor for classification of exposed areas.

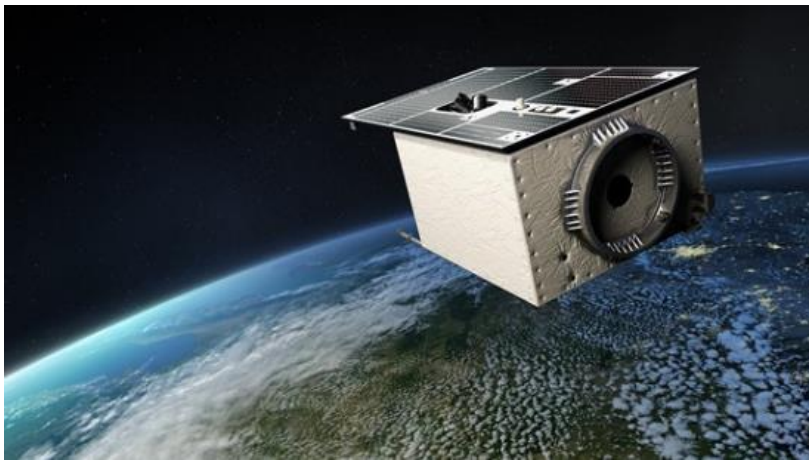

Fig. 8 Artist view of EnMAP satellite (DLR, 2012)

Fig. 9 Artist view of HySpIRI satellite (NASA, 2013)

Tab. 7 Lifetime of past-, present- and future-day sensors (multi-mode sensors are only mentioned on the highest spatial scale of analysis; for past- and present-day missions lifetimes are listed for the reference year 2012; for future missions expected mission

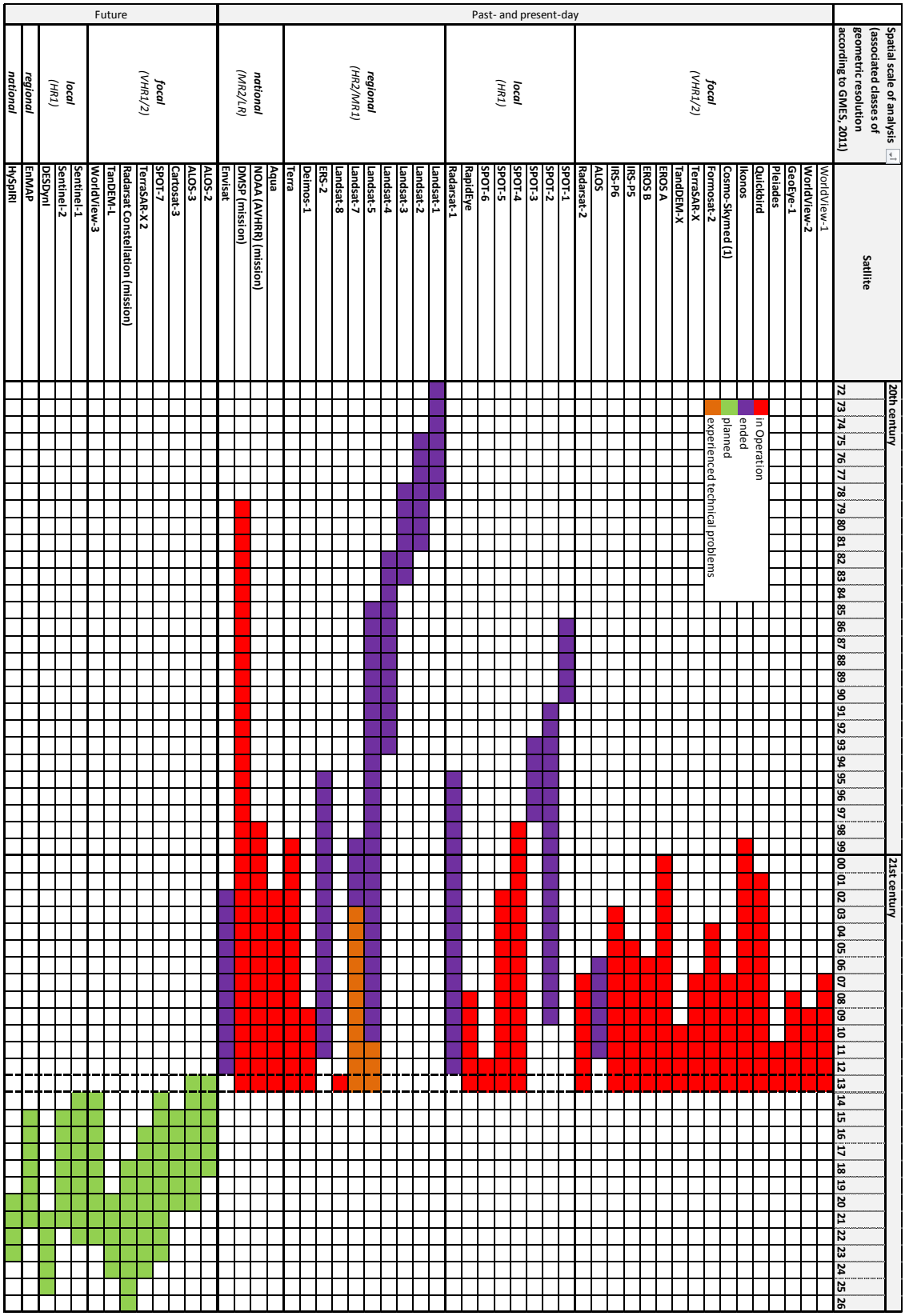

4. Remote sensing derived geo-products for exposure mapping

In the past decades international research groups from both government and academia have produced remote sensing derived geo-products that may provide valuable input to vulnerability-related research in the context of this project. These include on the one hand large-scale global or regional land cover datasets that can be used as a first approximation of human exposure as well as for the disaggregation of population census data. On the other hand, space-based pre-operational emergency preparedness and response services have produced a large product portfolio in recent years. A selection of products is put forward in the following subsections.

4.1 Land cover datasets

When a major disaster occurs, especially in remote parts of the world, knowing if the area is populated, and how densely, is crucial for the effective organisation humanitarian operations. This can help to reduce risks in areas that experience recurrent disasters and to focus post-disaster humanitarian interventions on the most likely populated places in disaster-affected countries and regions. In this context, global and regional land cover datasets present a valuable basis for the analysis of large-scale human exposures and a first approximation of their spatial distribution. Subsequently two data sets of regional European coverage as well as three data sets of global coverage are presented that could be used within in the project for the large-scale mapping of exposures and evaluation of project outputs and methodologies in terms of a systematic accuracy assessment.

The pan-European **CORINE Land Cover (CLC)** database provides a unique and comparable data base of seamless land cover and land use information for Europe based on satellite remote sensing images on a scale of 1:100,000 for the years 1990, 2000 and 2006. The most recent update was completed in 2010 and comprises 44 land use classes of which two correspond to urban fabric (continuous and discontinuous). With the regard to the multi-temporal approach, also area-wide regional land use change maps were obtained (DLR, 2011). The main data source for the production of the dataset were two European coverages of the Image 2006 dataset acquired by SPOT 4, SPOT 5 and IRS-P6 satellites from 2005 to 2007 provided by ESA. Land cover derivation was based on techniques of computer-aided photointerpretation and manual digitizing. While the evaluation of CLC 2006 accuracy is still under investigation, CLC 2000 was found to be 85 % thematically correct (EEA, 2006).

Featuring a more differentiated urban thematic detail, the **Urban Atlas** provides pan-European hot spot mapping of urban functional areas, on the basis of repeatedly and homogenously processed data for larger European cities (Seifert, 2009) and claims for

itself to be the first large-scale geo-data set ever produced operationally from higher resolution optical satellite data (Steinborn, 2009). The European Environment Agency (EEA) produced the detailed database of maps and land cover information for 117 European cities. It encompasses 22 urban thematic classes and four non-urban classes with a minimum mapping unit for all classes of 0.25 ha (Seifert, 2009). Information about impervious surfaces (IS), i.e. surfaces impenetrable by water as such as sidewalks, driveways, rooftops and parking lots as indicator for urban functional land use, are aggregated in five classes on building block level, ranging from discontinuous very low (<10% IS), low (>10-30% IS), medium (>30-50% IS) and dense (>50-80% IS) urban fabric to continuous urban fabric (> 80% IS) (Geiß et al., 2011). An overall thematic accuracy of 80% and 85% for the level 1 thematic class “Artificial surfaces” was determined (EC, 2012).

GlobCover is an ESA initiative which began in 2005 aiming at the provision of a global multi-class composite of land cover maps. Input EO data was acquired by the 300m MERIS sensor on board the ENVISAT satellite mission and processed mainly using techniques of unsupervised classification. ESA disseminated the land cover database comprising 22 classes, one of which describes artificial surfaces and associated areas, for two periods: December 2004 - June 2006 and January - December 2009 (ESA, 2011). Based on a limited number of reference samples a thematic overall accuracy of 73% was determined by Defourny et al. (2009).

The Joint Research Centre’s (JRC) **Global Human Settlement Layer (GHSL)** is a planned globally available urban land cover dataset realized as an on-going project since 2010 by the European Commission. For its derivation a novel approach has been developed to map, analyse and monitor human settlements and their spatiotemporal evolution in an automated manner. The GHSL automatic image information extraction workflow integrates multi-resolution (0.5m-10m) multi-platform, multi-sensor (PAN, multispectral), and multi-temporal image data. Multi-scale urban parameters such as built-up area and density as well as average size and number of buildings will be derived on spatial units of 10m, 50m and 500m. The first release of data in 2012 builds on over 16,000 remote sensing datasets covering over 24,000,000 km² from various sensors such as Ikonos, RapidEye, WorldView or SPOT also incorporating external datasets such as LandScan or MODIS500 for data-poor regions (JRC, 2011).

Based on the German space missions TSX and TDX two coverages of the entire landmass for 2011 and 2012 have been acquired. In this context, DLR has developed a pixel-based classification approach aiming to globally extract urban and non-urban structures from single radar imagery. The intended “**global urban footprint**” will be a binary classification of urban and non-urban areas at global scale based on single polarized images acquired in Stripmap mode with a resolution of approximately 3 × 3 m. Considering the challenges of a global urban footprint production, the algorithm is currently further investigated for the potential to improve the classification performance by substituting the presented threshold-based technique by a machine-learning approach (Esch et al., 2012). In a pilot study Taubenböck et al. (2011) used a pattern-based ac-

curacy assessment to evaluate classification results for the test case of Paddang, Indonesia, reaching an overall classification accuracy of 77%.

Further urban land cover data sets and related products such as **DMSP-OLS nighttime lights** or the **LandScan** population data set are listed in table 6. Derivation of the datasets is either image-based (e.g. **MOD500**, **GLOBC**, **GLC00**), based on combination of EO data and ancillary mapping products and census data (e.g. **IMPSA**, **LSCAN**, **HYDE3**, **GRUMP**), or originate entirely from external map products (e.g. **VMAP0**). Potere and Schneider (2009) give a thorough review of the described datasets and quantitatively compare the datasets by pairwise comparison, thus achieving a relative accuracy assessment in the form of contingency tables. However, absolute accuracies of these global and regional data sets are more difficult to assess and a stronger understanding of each map's strength and weakness is still on demand. With regard to the project at hand, DLR will provide a quantitative evaluation and systematic cross-validation of the presented products in WP6.

A novel undertaking for the generation of an open and homogenized global building and population inventory is the Global Exposure Database (GED) in the context of the public private partnership project Global Earthquake Model (GEM) (together **GED4GEM**) (GEM-NEXUS, 2013). The database is intended to be used in combination with hazard and vulnerability components to enable earthquake risk assessment for any part of the world. In this manner, the GED4GEM project consortium will collect, homogenize, and build upon many existing global or regional databases at different spatial scales (country-level, sub-country level, local scale and scale of individual buildings) to create this inventory in an ongoing project. Input data groups in this regard are global GIS vector layers (such as Open StreetMap, VMAP0, etc.), remote sensing and raster fusions data sets, demographic survey and census data or commercial databases (Huyck et al., 2011). As an ongoing project, the GED will be constantly updated during the project lifetime by the GEM community.

Tab. 8 Overview of global and regional urban land cover maps and related products including producer, reference/weblink (blue: weblinks for data access given in the reference list), input data used for derivation, most recent reference year, spatial and thematic resolution (updated and extended from Potere & Schneider, 2009)

Category	Map / Product	Producer / Refernce	Reference / Weblink	Specifiction / Source	Geomtric resolution	Reference Years	Thematic resolution
Land cover	**Vecor MAP Level Zero (VMAP0) (NIMA, 2005)**	US National Geospatial Intelligence Agency (US)	NIMA, 2005	Maps / Charts, City Gazetters	Scale 1:100,000	1997	10 thematic vector features including built-up areas
	Global Land Cover 2000 (GLC2000)	EC Joint Research Centre (JRC)	JRC, 2010	Landsat, SPOT-4 Vegetation Programme, VMAP0	32'' (~ 1km)	2000	22 themtic classes including one urban class
	History Database of the Global Environment (HYDE3)	PBL Netherlands Environmental Assessment Agency	PBL, 2011	UN census, VMAP0, GLC00, LandScan	5' (~ 10km)	1999/2000	global fraction of urban land (km²/gridcell)
	Global Impervious Surface Area (IMPSA)	Earth Observation Group, US National Geophysiscal Data Center (NGDC)	NGDC, 2010a	Landsat, Nighttime lights, LandScan	30'' (~ 1km)	2000/20001	global fraction of urban land (%)
	MODIS Urban Land Cover 500m (MOD500)	Center for Sustainability and the Global Environment (SAGE) - University of Wisonsin and Boston University (US NASA)	SAGE, 2013	MODIS 500m, Landsat, Maps / Charts	~ 500m	2001/2002	17 thematic classes including one urban class
	CORINE Land Cover	European Environment Agency (EEA)	EEA, 2012	IMAGE 2006 (SPOT 4 / 5, IRS P6 LISS3)	100m	2006	44 thematic classes including two urban classes
	European Urban Atlas	European Environment Agency (EEA)	EEA, 2010	VHR EO data (Spot-5, Quickbird, RapidEye, ALOS), Topographic maps, Road vectors, Soil Sealing data, Ancillary maps / charts	Scale 1:100,000 Mimimum mapping unit 0.25ha	2006	22 thematic urban classes (4 non-urban classes)
	GlobCover (GLOBC)	EC Joint Research Centre (JRC)	ESA, 2011	MERIS 300m, Maps / Charts, Road vectorsm GLC2000	~ 300m	2005	22 thematic classes including one urban class
	Global Rural-Urban Mapping Project (GRUMP)	NASA Socioeconomic Data and Applications Center (SEDAC) – Hosted by CIESIN at Columbia University	SEDAC, 2013	Nighttime lights, UN census, VMAP0, GLC00, LandScan	30'' (~ 1km)	2000	Binary (urban/rural)
	Global Urban Footprint (GUF)	German Remote Sensing Data Centre	-	TerraSAR-X	75m	2011/2012	Binary (urban/rural)
	Global Human Settlement Layer (GHSL)	EC Joint Research Centre (JRC)	JRC, 2012	HR EO data, open vector data (e.g. Open StreemapSM), census data	10 / 50 / 500m	ongoing	Subpixel information: - built-up are (m²) - built-up percentage (%) - average building size (m²) - building number
Nitghttime Lights	**DMSP-OLS Nighttime Lights (LITES)**	Earth Observation Group, US National Geophysiscal Data Center (NGDC)	NGDC, 2010b	DMSP-OLS	30'' (~ 1km)	2010	Nighttime ilumination intensity
Population	**LandScan (LSCAN)**	US Oak Ridge National Laboratory (ORNL)	ORNL, 2011	HR EO data (e.g. from Landsat), US census, Maps / Charts, City Gazetters, Road Vectors, VMAP1, MOD1K	30'' (~ 1km)	2011	Ppl./km²

Based on the prospect of mission presented in chapter 3, future remote sensing data sets hold a great potential for the global and regional mapping of land cover as an indicator for human and physical exposure. Providing enhanced geometric resolutions, thematic details, frequent revisit times and mostly area-wide monitoring capabilities many of these data are suitable for the generation of large-scale and thematically more detailed land cover inventors. For example, the ESA's Sentinel-1 and Sentinel-2 missions feature both spatial and thematic capabilities for the generation of such data-

bases. Radarsat-2 data was already successfully tested for transfer of urban land cover classification methodology from TSX data by Taubenböck et al. (2012). Thus, the Constellation satellites with their enhanced capabilities are very promising systems with regard to radar-based urban mapping. In this context, also the German follow-up mission TSX 2 featuring a significantly improved spatial resolution is predestinated to continue the process of mapping the global urban footprint. Beyond that, the fusion with data from hyperspectral systems like EnMAP and HyspIRI holds great potential for a thematic differentiation of urban built-up classes. On the smaller scale of urban morphology the enhanced availability of very high and high resolution optical and stereo data from satellites such as Cartosat-3 or WorldView-3 will add to inventories of 3D city models.

4.2 Emergency preparedness and response products

GMES is a joint initiative of the European Commission and ESA aiming at achieving an autonomous and operational Earth observation capacity (ESA, 2013). In this context, pre-operational applications of disaster-related mapping services have been demonstrated in multidisciplinary pre-cursor projects within the European Commission Framework Program, mainly aiming at near real-time emergency response services or early warning applications to establish operational service for emergency preparedness and response. Projects associated in this context are SAFER (FP7; SAFER, 2011), LinkER (FP7; LinkER, 2012) and G-MOSAIC (FP7; G-MOSAIC 2012) and will be presented in the following. Within these frameworks, remote sensing plays a crucial role as source of information for multiple hazards in rapid mapping and emergency response applications (Geiß & Taubenböck, 2012).

SAFER is a European Commission FP7 research programme lead by DLR that started in January 2009 with the aim to provide pre-operational GMES emergency response services by the employment of a fully operational EO-based segment. In the context of SAFER, a user-friendly space-based geo-information product portfolio has been developed covering a vast range of mapping products supporting civil protection and humanitarian aid during the whole disaster management cycle. Products are made publicly available via two temporal modes of dissemination: Post-event emergency response rapid mapping products are delivered in rush mode within 8 hours of data reception, whereas all other products relating to pre-event preparedness and prevention as well as post-event recovery monitoring are produced as emergency support products within two to nine weeks after data reception. In this manner, the centre for satellite-based crisis information (DLR-ZKI) covered several disaster types such as meteorologically-driven hazards (e.g. fires, floods), geophysical hazards (e.g. earthquakes, volcanic eruptions, landslides), man-made disasters (e.g. technical incidents) as well as humanitarian disasters in more than 70 emergency activations (DLR, 2013) providing a product portfolio ranging from large-scale to detailed geographic reference maps describing location and extent of hazards as well as change detection-based damage assessment maps. In this context, project **LinkER** (LinkER 2012) explicitly supports the implementation and use of operational service developed in SAFER as a preparatory action across the whole European Union. The project's main aim is to put an operational infrastructure for services in place by customization of tools, data dissemination,

integration and automation of data workflows as well as training and exercise for end-users.

G-Mosaic is a further project aiming at the development of pre-operational services across five key domains of risk management including nuclear and treaty monitoring, natural resources and conflicts, migration and border monitoring, critical assets as well as crisis management and assessment (G-MOSAIC, 2012). Herein the main aim is to provide the European community with geospatial intelligence for preparedness-related applications of crisis prevention and early warning as well as crisis management and intervention. In this context, G-MOSAIC has elaborated a wide EO-based product portfolio in each of the thematic domains. With regard to crisis management for example, rapid geospatial reporting covers EO-derived products spanning from geographic reference maps, rapid damage assessment, radar-based change detection, activity analysis, evacuation support to analysis of critical infrastructure.

Overall, the presented applications have demonstrated the potential of remote sensing for operational mapping applications in the post- and preparation phases as an area-wide, independent and up-to-date data basis for multiple hazards in rapid mapping and response. Future remote sensing missions presented in chapter 3 featuring increased geometric and thematic detail as well as higher revisit capabilities and area-wide availability will foster existent applications of disaster preparedness, early warning and emergency response. In terms of earthquake and landslide preparedness and early warning, for example, TDL will open up opportunities to better understand the earth's dynamic surface processes and will improve overall hazard prediction capabilities in the long term. Furthermore, NASA's DESDynI mission is meant to meet the geodetic measurement precision of interferometric SAR technologies to accurately map surface deformations and thus enhance the predictive determination of earthquake and landslide likelihoods. Furthermore, systems such as Setinel-2 will provide frequent imagery of hazard events such as landslides, volcanic eruptions, and floods which will add to the product portfolio of post-event emergency response services such as reference maps, spatial damage assessment and determination of affected areas and infrastructure.

5. Conclusion

Undertakings for integrative and comprehensive risk analysis commonly encounter the problems of an appropriate data collection. Shortcomings of available data include that data sources are often too generalized, outdated, inconsistent or simply not available. In this context, remote sensing is generally perceived as a promising tool for an economical, up-to-date and independent data collection and has been employed in various investigations in the geo-risk context. In this regard, the review of applications in *chapter 1* emphasises the versatility of remote sensing data and techniques with regard to the analysis of earthquake and landslide risks, both for hazard- and vulnerability-centred investigations.

Geometric resolution of remote sensing systems, their scene size and thus, the spatial scale of analysis, need always be selected in consideration of the objects to be analysed. Data from past- and present-day sensors presented in *chapter 2* with a coarse geometric resolution and larger aerial coverage enable overall evaluation of pre- and post-event situations are often freely available. On the contrary, data availability from VHR systems such as airborne LIDAR or VHR optical data over larger areas affected for in-depth analysis is still limited due to high costs. Future earth observation missions presented in *chapter 3* have the potential to play a key role in earthquake- and landslide-related investigations and to continue or even improve geoinformation products in the near future. For example, the ESA Sentinel missions will feature enhanced geometric and thematic capabilities and increased revisit capabilities at low cost and will further provide data continuity as several past- and present-day mission will reach the end of their technical lifetime. In this context, the enhanced capabilities of the described missions are believed to enable a leap forward in earthquake and landslide risk research both for hazard- as well as vulnerability-related investigations. However, the limiting factor of data cost yet needs to be assessed.

Apart from the perspective on future mission, international research groups have produced remote sensing based geo-products put forward in *chapter 4* that will provide valuable input to vulnerability-related research of the project at hand. On the one hand, space-based pre-operational emergency response services have produced a large product portfolio and significant experiences in post-event mapping applications in recent years. On the other hand, both large- scale global or regional land cover inventories that will be used as a first approximation of human and physical exposure have been produced. Nevertheless, a better understanding of each data set’s strength and weakness is still on demand and DLR will provide a quantitative evaluation and systematic cross-validation of the presented products in WP6.

Overall, from a technical perspective, the constantly increasing availability and accessibility of modern-day remote sensing technologies and the enhanced technical capabilities of future missions will provide new opportunities and data continuity for a wide range of geo-risk investigations.

References cited

Aubrecht, C., Özceylan, D., Steinnocher, K., Freire, S. (2012) Multi-level geospatial modeling of human exposure patterns and vulnerability indicators. In: Taubenböck, H., Post, J., Strunz, G. (eds) Remote sensing contributing to mapping earthquake vulnerability and effects. Special Issue in Natural Hazards.

Aydöner, C., Maktav, D. (2009) The role of the integration of remote sensing and GIS in land use/land cover analysis after an earthquake. International Journal of Remote Sensing, 30, 1697–1717.

Berger, M., Aschbacher, J. (2012) Preface: the sentinel missions-new opportunities for science. Remote Sensing of Environment, 120, 1-2.

Birkmann, J. (2006) Indicators and criteria for measuring vulnerability: theoretical bases and requirements. In: Birkmann, J. (ed.) Measuring vulnerability to natural hazards. United Nations University Press, New York, 55–77.

Bohle, H.G. (2001) Vulnerability and criticality perspectives from social geography. IHDP Update 2/2001. Global Environmental Change, 2, 1–7.

Borfecchia, F., Pollino, M., De Cecco, L., Lugari, A., Martini, S., La Porta, L., Ristoratore, E., Pascale C (2010) Active and passive remote sensing for supporting the evaluation of the urban seismic vulnerability. Italian Journal of Remote Sensing, 42,129–141.

Borzi, B., Dell'Acqua, F., Faravelli, M., Gamba, P., Lisini, G., Onida, M., Polli, D. (2011) Vulnerability study on a large industrial area using satellite remotely sensed images. Bulletin of Earthquake Engineering, 9, 675–690.

Brunner, D., Lemoine, G., Bruzzone, L. (2010) Earthquake damage assessment of buildings using VHR optical and SAR imagery. IEEE Transactions on Geoscience and Remote Sensing, 48, 2403–2420.

Cartwright, S. (2005) National Civil Defence Emergency Management Plan Order 2005. Published under the authority of the New Zealand Government, Wellington, New Zealand, 68 pp.

CEOS (2012) CEOS mission, instruments and measurements database online. Available at http://database.eohandbook.com/ Accessed 23 Jun 2013

Chang, L., Tang, Z. (2010) Using remote sensing technology to assess land—use changes after the Northridge Earthquake. Disaster Advances, 3, 5–10.

Chen, K. (2002) An approach to linking remotely sensed data and areal census data. International Journal of Remote Sensing, 23, 37–48.

Chiroiu, L., Adams, B., Saito, K. (2006) Advanced techniques in modeling, response and recovery. In: Oliveira, C.S., Roca, A., Goula, X. (eds.) Assessing and managing earthquake risk. Springer, Dordrecht, 427–448.

Chuvieco, E., Huete, A. (2010) Fundamentals of satellite remote sensing. Boca Raton: CRC Press.

CRISP (2001) Optical Remote Sensing. Available at http://www.crisp.nus.edu.sg/~research/tutorial/optical.htm 5 Jul 2013

CSA (2012) Canadian space agency—RADARSAT Mission description. Available at http://www.asc-csa.gc.ca/eng/satellites/radarsat/description.asp Accessed 11 Jun 2013

Cunningham, D., Grebby, S., Tansey, K., Gosar, A., Kastelic, V. (2006) Application of airborne LiDAR to mapping seismogenic faults in forested mountainous terrain, southeast Alps, Slovenia. Geophysical Research Letters, 33, L20308.

Dech, S. (1997) Anwendung der Satellitenfernerkundung. Von der geowissenschaftlichen Forschung zum operationellem Einsatz. DLR Forschungsbericht, 97, 52.

Defourny, P., Schouten, L., Bartalev, S., Bontemps, S., Caccetta, P., de Witt, A., di Bella, C., Gerard, B., Giri, C., Gond, V., Hazeu, G., Heinimann, A., Herold, M., Jaffrain, G., Latifovic, R., Ling, H., Mayaux, P., Muncher, S., Nonguierma, A., Stibig, H-J., Van Bogaert, E., Vancutsem, C., Bicheron, P., Leroy, M. and Arino, O. (2009) Accuracy Assessment of a 300-m Global Land Cover Map: the GlobCover Experience. Proceedings of the 33rd International Symposium on Remote Sensing of Environment (ISRSE), Stresa, Italy, May 2009.

Deichmann, U., Ehrlich, D., Small, C., Zeug, G. (2011) Using high resolution satellite data for the identification of urban natural disaster risk. Global Facility for Disaster Reduction and Recovery, Washington, DC.

Dell'Acqua, F., Lisini, G., Gamba, P. (2009) Experiences in optical and SAR imagery analysis for damage assessment in the Wuhan, May 2008 Earthquake. IEEE International Geoscience and Remote Sensing Symposium, 1–5, 2417–2420.

DESDynI (2011) Deformation, ecosystem structure and dynamics of ice—mission concept. Available at http://desdyni.jpl.nasa.gov/mission/. Accessed 11 Jun 2013

DigitalGlobe (2012) WorldView-3. Available at http://www.digitalglobe.com/downloads/WorldView3-DSWV3-Web.pdf Accessed 11 Jun 2013.

Ding X, Huang W (2011) D-InSAR monitoring of crustal deformation in the eastern segment of the Altyn Tagh Fault. International Journal of Remote Sensing, 32,1797–1806.

DLR (2010) TanDEM-X Science Home – Mission goal. Available at http://www.dlr.de/hr/en/desktopdefault.aspx/tabid-2317/3669_read-5492/ Accessed: 26 Jun 2013

DLR (2011) Corine Land Cover – Germany. Available at http://www.corine.dfd.dlr.de/intro_en.html Accessed 14 Jun 2013

DLR (2012) EnMap – Germany's hyperspectral satellite for Earth Observation. Available at http://www.dlr.de/dlr/en/desktopdefault.aspx/tabid-10379/567_read-421/#gallery/2671 Accessed 11 Jun 2013 Accessed 14 Jun 2013

DLR (2013) DLR-ZKI successful activities within the GMES emergency responser service. Available at http://www.zki.dlr.de/de/gmes-ers Accessed 11 Jun 2013

Dobson J.E., Bright, E.A., Coleman, P.R., Durfee, R.C., Worley, B.A. (2000) LandScan: a global population database for estimating populations at risk. Photogrammetric Engineering and Remote Sensing, 66, 849–857.

Ebert, A., Kerle, N., Stein, A. (2009) Urban social vulnerability assessment with physical proxies and spatial metrics derived from air- and spaceborne imagery and GIS data. Natural Hazards, 48, 275–294.

EC (2012) Mapping Guide – for a European Urban Atlas. Available at ec.europa.eu/regional_policy/tender/pdf/2012066/annexe2.pdf Accessed 14 Jun 2013.

EEA (2006) Corine land cover database passes accuracy test. Availble at: http://www.eea.europa.eu/highlights/Ann1151398593 Accessed 14 Jun 2013

EEA (2010) Urban Atlas. Available at: http://www.eea.europa.eu/data-and-maps/data/urban-atlas Accessed 10 Jul 13

EEA (2012) Corine Land Cover 2006 seamless vector layer. Available at: http://www.eea.europa.eu/data-and-maps/data/clc-2006-vector-data-version-2 Accessed 10 Jul 13

Eguchi, R.T., Huyck, C.K., Adams, B.J., Mansouri, B., Houshmand, B., Shinozuka, M. (2003) Resilient disaster response: using remote sensing technologies for post-earthquake damage detection. MCEER Research Progress and Accomplishments, 2001–2003.

Ehrlich, D., Zeug. G., Gallego, J., Gerhardinger, A., Caravaggi, I., Pesaresi, M. (2010) Quantifying the building stock from optical high-resolution satellite imagery for assessing disaster risk. Geocarto International, 25(4), 281–293.

Eicher, C.L., Brewer, C.A. (2001) Dasymetric mapping and areal interpretation interpolation: implementation and evaluation. Cartography and Geographic Information Science, 28, 125-138.

Eineder, M., Friedrich, A., Minet, C., Bamler, R., Flerit, F., Hajnsek, I. (2009) Scientific requirements and feasibility on an L-band mission dedicated to measure surface deformation. IEEE International Geoscience and Remote Sensing Symposium. 12–17 July 2009, Cape Town, South Africa.

eoPortal (2013) Satellite Missions Database. Available at: https://directory.eoportal.org/web/eoportal/satellite-missions Accessed 11 Jun 2013

ESA (2011) GlobCover Available at http://due.esrin.esa.int/globcover/ Accessed 10 Jul 13

ESA (2011) GlobCover. Available at: http://due.esrin.esa.int/globcover/ Accesse 14 Jun 2013

ESA (2012) Deimos-1. Available at: at: https://earth.esa.int/web/guest/missions/3rd-party-missions/current-missions/deimos-1 23 Jun 2013

ESA (2013) European Space Agency – ESA's Sentinel satellites: Overview, Sentinel-1,

Sentinel-2. Available at http://www.esa.int/Our_Activities/Observing_the_Earth/GMES/Sentinel-1 Accessed 11 Jun 2013 Accessed 11 Jun 2013

Esch, T., Dech, S., Roth, A., Schmidt, M., Taubenböck, H., Heldens, W., Thiel, M., Wurm, M., Klein, D. (2009) Monitoring and assessment of urban environments using space-borne earth observation data. In: Kreck, A., Rumor, M., Zlatanova, S., Fendel, E. (eds) Urban and regional data management. Taylor & Francis Group, London, 385–398.

Esch, T., Taubenböck, H., Roth, A., Heldens, W., Felbier, A., Thiel, M., Schmidt, M., Müller, M., Müller, A., Dech, S. (2012) TanDEM-X mission—new perspectives for the inventory and monitoring of global settlement patterns. Journal of Applied Remote Sensing, 6, 061702.

Fielding, E.J., Wright, T.J., Muller, J., Parsons, B.E., Walker, R. (2004) Aseismic deformation of a fold-and-thrust belt imaged by synthetic aperture radar interferometry near Shahdad, southeast Iran. Geology, 32, 577–580.

French S.P., Muthukumar, S. (2006) Advanced technologies for earthquake risk inventries. Journal of Earthquake Engineering, 10, 207–236.

Fu, B., Ninomiya, Y., Lei, X., Toda, S., Awata, Y. (2004) Mapping active fault associated with the 2003 Mw 6.6 Bam (SE Iran) earthquake with ASTER 3D images. Remote Sensing of Environment, 92, 153–157.

Gamba, P., Houshmand, B., (2002) Joint analysis of SAR, LIDARand aerial imagery for simultaneous extraction of land cover, DTM and 3D shape of buildings. International Journal of Remote Sensing, 23, 4439– 4450.

Ge, Y., Xu, J., Liu, Q., Yao, Y., Wang, R. (2009) Image interpretation and statistical analysis of vegetation damage caused by the Wenchuan earthquake and related secondary disasters. Journal of Applied Remote Sensing, 3:031660.doi:10.1117/1.3141726 (26 May 2009).

Geiß, C., Taubenböck, H. (2012) Remote sensing contributing to assess earthquake risk: from a literature review towards a roadmap. Natural Hazards, 1-42. doi: 10.1007/s11069-012-0322-2.

Geiß, C., Taubenböck, H., Wurm, M., Esch, T., Nast, M., Schillings, C., Blaschke, T. (2011) Remote Sensing-Based Characterization of Settlement Structures for Assessing Local Potential of District Heat. Remote Sensing 3, 1447–1471.

Geiß, C., Wurm, M., Taubenböck, H., Heldens, W., Esch, T. (2011) Comparison of selected impervious surface products derived from remote sensing data. In: Proceedings of the JURSE 2011. Presented at the JURSE 2011, Munich.

GEM-NEXUS (2013) GED4GEM Exposure database. Available at: http://www.nexus.globalquakemodel.org/ged4gem/posts Accessed 8 Jul 13

GFZ (2012) EnMAP – Environmental Mapping and Analysis Program. Available at http://www.gfz-potsdam.de/portal/gfz/Struktur/Departments/Department+1/sec14/projects/enmap;jsessionid=8109B074FB80292C62335A5838A069EA Accessed 12 Jun

G-MOSAIC (2012) G-MOSAIC: GMES pilot services for security. Available at http://www.gmesgmosaic.eu/. Accessed 14 Jun 2013

Guo, H. (2010) Understanding global natural disasters and the role of earth observation. International Journal of Digital Earth, 3, 221–230.

Heldens, W., Heiden, U., Esch, T., Stein, E., Müller, A. (2011) Can the future EnMAP mission contribute to urban applications? A Literature Survey. Remote Sensing, 3, 1817–1846.

Hong, Y., Adler, R., Huffmann, G. (2007) Use of satellite remote sensing data in the mapping of global landslide susceptibility. Natural Hazards, 43, 245–256.

Huang, R.Q., Li, W.L. (2009) Analysis of the geo-hazards triggered by the 12 May 2008 Wenchuan Earthquake. China Bulletin of Engineering Geology and Environment, 68, 363–371.

Huber, S., Younis, M., Krieger, G. (2010) The TanDEM-X mission: Overview and interferometric performance. International Journal of Microwave and Wireless Technologies, 2, 379-389.

Huyck, C., Esquivias, G., Gamba, P., Hussain, M., Odhiambo, O., Jaiswal, K., Chen, B., Yetman, G. (2011) Survey of available input databases for GED. Deliverable 2.2. Global Exposure Database for the Global Earthquake Model (GED4GEM). Avilable at: http://www.nexus.globalquakemodel.org/ged4gem/posts/ged4gem-deliverable-d2.2-survey-of-available-input-databases-for-ged Accessed 9 Jul 2013

Imhoff, M.L., Lawrence, W.T., Stutzer, D.C., Elvidge, C.D. (1997) A technique for using composite DMSO/OLS `city lights' satellite data to map urban area". Remote Sensing of Environment, 361-370.

Janoth, J., Gantert, S., Koppe, W., Kaptein, A., Fischer, C., 2012. TerraSAR-X2 - Mission overview. IEEE, pp. 217–220.

JAXA (2011) Advanced land observing satellite-2. Available at http://www.jaxa.jp/projects/sat/alos2/index_e.html. Accessed 11 Jun 2013

Jensen, J.R. (2007) Remote Sensing of the Environment: An Earth Resource Perspective. London: Pearson Prentice Hall.

Joyce, K., Wright, K., Samsonov, S. (2009b) Remote sensing and the disaster management cycle. In: Jedlovec, G. (ed) Advances in geoscience and remote sensing, vol. 48(7). INTECH, pp 317–346.

Joyce, K.E., Belliss, S.E., Samsonov, S.V., McNeill, S.J., Glassey, P.J. (2009a) A review of the status of satellite remote sensing and image processing techniques for mapping natural hazards and disasters. Progress in Physical Geography, 33, 183–207.

JRC (2010) Global Land Cover 2000. Available at http://bioval.jrc.ec.europa.eu/products/glc2000/products.php Accessed 10 Jul 13

JRC (2012) Global Human Settlement Layer. Available at: http://ghslsys.jrc.ec.europa.eu/ Accessed 14 Jun 2013.

Kaab, A. (2002) Monitoring high-mountain terrain deformation from repeated air- and

spaceborne optical data: examples using digital aerial imagery and ASTER data. ISPRS Journal of Photogrammetry and Remote Sensing, 57, 39–52.

Katti, R.V., Thyagarajan, K., Shankara, N.K., Kiran Kumar, S.A. (2007) Spacecraft technology, special section: Indian space programme. Current Science, 93, 1715–1736.

Kerle, N. (2010) Satellite-based damage mapping following the 2006 Indonesia earthquake—how accurate was it? International Journal of Applied Earth Observation and Geoinformation, 12, 466–476.

Krieger, G., Hajnsek, I., Papathanassiou, K., Eineder, M., Eineder, M., Younis, M., De Zan, F., Prats, P., Huber, S., Werner, M., Fiedler, H., Freeman, A., Rosen, P., Hensley, S., Johnson, W., Veilleux, L., Grafmüller, B., Werninghaus, R., Bamler, R., Moreira, A. (2009) *The Tandem-L Mission Proposal: Monitoring Earth's Dynamics with High Resolution SAR Interferometry.* In: Proceedings of the IEEE Radar Conference (RadarCon) (DOI: 10.1109/RADAR.2009.4977077), 1-6.

Langford, M., Higgs, G., Radcliffe, J., White, S. (2008) Urban population duistribution models and service accessibility estimation. Computers, Environment and Urban Systems, 32, 66-80.

Li, M., Cheng, L., Gong, J., Liu, Y., Chen, Z., Li, F., Chen, G., Chen, D., Song, X. (2008) Post-earthquake assessment of building damage degree using LiDAR data and imagery. Science China Series E: Technology Science, 51, 133–143.

Lin, W.T., Chou, W.C., Lin, C.Y. (2008) Earthquake-induced landslide hazard and vegetation recovery assessment using remotely sensed data and a neural network-based classifies: a case study in central Taiwan. Natural Hazards, 47, 331-347.

Lindell, M.K. (2000) Politics of hazard mitigation. Natural Hazards Review, 1(2), 73-82.

LinkER (2012) linkER-supporting the implementation of operational GMES services in emergency response. Available at http://www.zki.dlr.de/project/1394. Accessed 14 Jun 2013

Mantovani, F., Soeters, R., van Westen, C.J. (2013) Remote sensing techniques for landslide studies and hazard in Europe. Geomorphology, 14, 213-225.

Martha, T.R., Kerle, N., van Westen, C.J., Jetten. V., Kumar, K.V. (2011) Segment optimization and data-driven thresholding for knowledge-based landslide detection by object-based image analysis. IEEE Transactions on Geoscience and Remote Sensing, 49, 4928–4943.

Massonnet, D., Feigl, K. (1998) Radar interferometry and its application to changes on the earth surface. Reviews of Geophysics, 36, 441–500.

Mennis, J., Hultgren, T. (2006) Intelligent daysmetric mapping and its application to aeal interpolation. Cartography and Geographic Information Science, 33, 179-194.

Mensah, E.M. (2009) Lidar Techniques and Remote Sensing in the Atmosphere: Understanding the Use of Laser Light in the Atmosphere. Bloomington, IN: Author House.

Mileti, D. (1999) Disasters by Design: A Reassessment of Natural Hazards in the United

States. Washington, D.C.: Joseph Henry Press.

Minet, C., Eineder, M., Bamler, R., Hajnsek, I., Friedrich, A. (2008) Requirements for an L-band SAR-Mission for global monitoring of tectonic activities. USEReST '08, 11–14 November 2008, Naples, Italy.

MODIS500 (2013) Global maps of urban extent from satellite data. Available at http://sage.wisc.edu/people/schneider/research/data.html Accessed 10 Jul 13

Moreira, A., Krieger, G., Younis, M., Hajnsek, I., Papathanassiou, K., Eineder, M., De Zan, F. (2011) Tandem-L: a mission proposal for monitoring dynamic earth processes. In: IEEE international geoscience and remote sensing symposium, 25–29 July 2011, Vancouver, Canada.

Mueller, M., Segl, K., Heiden, U., Kaufmann, H. (2006) Potential of high-resolution satellite data in the context of vulnerability of buildings. Natural Hazards, 38, 247–258.

NASA (2013) HyspIRI Mission Study Website. Available at http://hyspiri.jpl.nasa.gov/ Accessed 11 Jun 2013

Neer, J.T. (1999) High resolution imaging from space—a commercial perspective on a changing landscape. International Archives of Photogrammetry and Remote Sensing, XXXII(7C2):132-143.

NGDC (2010) Global Distribution and Density of Constructed Impervious Surfaces Available at http://ngdc.noaa.gov/eog/dmsp/download_global_isa.html Accessed 10 Jul 13

NGDC (2010) Version 4 DMSP-OLS Nighttime Lights Time Series. Available at http://ngdc.noaa.gov/eog/dmsp/downloadV4composites.html Accessed 10 Jul 13

NIMA (2005) VMAP0. Available at http://www.mapability.com/index1.html?http&&&www.mapability.com/info/vmap0_download.html Accessed 10 Jul 13

ORNL (2011) Landscan. Available at http://www.ornl.gov/sci/landscan/ Accessed 10 Jul 13

Ostir, K., Veljanovski, T., Podobnikar, T. and Stancic, Z. (2003) Application of satellite remote sensing in natural hazard management: the Mount Mangart landslide case study. International Journal of Remote Sensing, 24, 3983–4002.

Parkinson, C. L., Greenstone, R. (2000) EOS data products handbook, Volume 2, NASA Goddard Space Flight Center, Greenbelt, Maryland, USA.

Paul, B.K. (2011) Environmental Hazards and Disasters: Contexts, Perspectives and Management. Chichester: Wiley-Blackwell.

PBL (2011) History Database of the Global Environment. Available at: http://themasites.pbl.nl/tridion/en/themasites/hyde/download/index-2.html Accessed 10 Jul 13

Philip, G. (2010) Remote sensing data analysis for mapping active faults in the northwestern part of Kangara Valley, NW Himalaya, India. International Journal of Remote Sensing, 28(21), 4745–4761.

Pittore, M., Wieland, M. (2019) Towards a rapid probabilistic seismic vulnerability

assessment using satellite and ground-based remote sensing. Natural Hazards, doi: 10.1007/s11069-012-0475-z, 2012.

Potere, D., Schneider, A. (2009) Comparison of global urban maps, In: Global mapping of Human Settlement, In: Gamba, P. and M. Herold (Eds.), Global Mapping of Human Settlements: Experiences, Data Sets, and Prospects, Taylor and Francis, Boca Raton, FL.

Rathje, E.M., Adams, B.J. (2008) The role of remote sensing in earthquake science and engineering: opportunities and challenges. Earthquake Spectra, 24, 471–492.

Rejaie, A., Shinozuka, M., (2004) Reconnaissance of Golcuk 1999 earthquake damage using satellite images. Journal of Aerospace Engineering,. 17, 20– 25.

Roessner, S., Wetzel, H.U., Kaufmann, H., Sarnagoev, A. (2005) Potential of satellite remote sensing and GIS for landslide hazard assessment in Southern Kyrgyzstan (Central Asia). Natural Hazards, 35, 395–416.

Rott, H., Nagler, T. (2006) The contribution of radar interferometry to the assessment of landslide hazards. Advances in Space Research 37, 710–19.

SAFER (2011) Services and applications for emergency response. Available at http://safer.emergencyresponse.eu/site/FO/scripts/myFO_accueil.php?lang=EN. Accessed 14 Jun 2013

Sahar, L., Muthukumar, S., French, P. (2010) Using aerial imagery and GIS in automated building footprint extraction and shape recognition for earthquake risk assessment of urban inventories. IEEE Transactions in Geoscience and Remote Sensing, 48, 3511–3520.

Salvi, S., Stramondo, S., Funning, G.J., Ferretti, A., Sarti, F., Mouratidis, A. (2012) The Sentinel-1 mission for the improvement of the scientific understanding and the operational monitoring of the seismic cycle. Remote Sensing of Environment, 120, 164–174.

SEDAC (2013) Global Rural-Urban Mapping Project. Available at http://sedac.ciesin.columbia.edu/data/collection/grump-v1 Accessed 10 Jul 13

Seifert, F.M. (2009) Improving Urban Monitoring towards a European Urban Atlas. In: Gamba, P., Herold, M. (eds.), Global Mapping of Human Settlement. Experiences, Data sets, and Prospects, 2009, pp. 231-250.

Small, C. and Cohen, J. (2004). Continental physiography, climate, and the global distribution of human population. Current Anthropology, 45(2), 269–277.

Steinborn, W. (2010) The Europe Urban Atlas – supporting city habitability. Available at http://www.sensorsandsystems.com/article/features/6403-the-european-urban-atlas-supporting-city-habitability.html Accessed 14 Jun 2013

Stramondo, S., Moro, M., Tolomei, C., Cinti, F.R., Doumaz, F. (2005) InSAR surface displacement field and fault modelling for the 2003 Bam earthquake (southeastern Iran). Journal of Geodynamics, 40, 347–353.

Stumpf, A., Kerle, N. (2011) Object-oriented mapping of landslides using random forests. Remote Sensing of Environment, 115, 2564-2577.

Taubenböck, H. (2011) The vulnerability of a city—diagnosis from a bird's eye view. In: Mörner N.A. (ed) The Tsunami threat—research and technology. InTech, Croatia, pp 107–128.

Taubenbock, H., Esch, T., Felbier, A., Roth, A., Dech, S. (2011) Pattern-Based Accuracy Assessment of an Urban Footprint Classification Using TerraSAR-X Data. IEEE Geoscience and Remote Sensing Letters, 8, 278–282.

Taubenböck, H., Esch, T., Felbier, A., Wiesner, M., Roth, A., and Dech, S. (2012a) Monitoring urbanization in mega cities from space. Remote Sensing of the Environment, 117, 162-176.

Taubenböck, H., Felbier, A., Esch, T., Roth, A., Dech, S. (2012): Pixel-based classification algorithm for mapping urban footprints from radar data – a case study for RADARSAT-2. Canadian Journal of Remote Sensing, 38, 211-222.

Taubenböck, H., Post, J., Roth, A., Zosseder, K., Strunz, G., Dech, S. (2008) A conceptual vulnerability and risk framework as outline to identify capabilities of remote sensing. Natural Hazards and Earth System Sciences, 8, 409–420.

Taubenböck, H., Roth, A., Esch, T., Felbier, A., Müller, A., & Dech S. (2012b). The vision of mapping the global urban footprint using the TerraSAR-X and TanDEM-X mission. In: Zlatanova, Ledoux, Fendel & Rumor (eds.), *Urban and Regional Management*. Taylor & Francis Group, London, 243-251.

Taubenböck, H., Wurm, M., Netzband, M., Zwenzner, H., Roth, A., Rahman, A., Dech, S., (2011) Flood risks in urbanized areas – multi-sensoral approaches using remotely sensed data for risk assessment. Natural Hazards and Earth System Science, 11, 431–444.

Taubenböck. H., Goseberg, N., Setiadi, N., Lämmel, G., Moder, F., Oczipka, M., Klüpfel, H., Wahl, R., Schlurmann, T., Strunz, G., Birkmann, J., Nagel, K., Siegert, F., Lehmann, F., Dech, S., Gress, A., Klein, R. (2009) "Last-Mile" preparation for a potential disaster—interdisciplinary approach towards tsunami early warning and an evacuation information system for the coastal city of Padang, Indonesia. Natural Hazards and Earth System Sciences, 9, 1509–1528.

Theilen-Willige, B. (2010) Detection of local site conditions influencing earthquake shaking and secondary effects in Southwest-Haiti using remote sensing and GIS-methods. Natural Hazards and Earth System Sciences, 10, 1183–1196.

Tierney, K.J., Lindell, M.K., Perry, R.W. (2001) Facing the Unexpected. Disaster Preparedness and Response in the United States. Washington, D.C. Joseph Henry Press.

Torres, R., Snoeij, P., Geudtner, D., Bibby, D., Davidson, M., Attema, E., Potin, P., Rommen, B., Floury, N., Brown, M., Traver, I.N., Deghaye, P., Duesmann, B., Rosich, B., Miranda, N., Bruno, C., L'Abbate, M., Croci, R., Pietropaolo, A., Huchler, M., Rostan, F., 2012. GMES Sentinel-1 mission. Remote Sensing of Environment, 120, 9–24.

Tralli, D.M., Blom, R.G., Zlotnicki, V., Donnellan, A., Evans, D.E. (2005) Satellite remote sensing of earthquake, volcano, flood, landslide and coastal inundation hazards.

Journal for Photogrammetry and Remote Sensing, 59, 185-198.

Trianni, G., Gamba, P. (2009) Fast damage mapping in case of earthquakes using multitemporal SAR data. Journal of Real-Time Image Processing, 4, 195–203.

Tronin, A.A. (1996) Satellite thermal survey—a new tool for the study of seismoactive regions. International Journal of Remote Sensing, 17(8), 1439–1455.

Tronin, A.A. (2006) Remote sensing and earthquakes: A review. Physics and Chemistry of the Earth, 31, 138-142.

Tronin, A.A. (2010) Satellite remote sensing in seismology. A review. Remote Sensing, 2, 124–150.

Tsai, Y.B., Liu, J.Y., Ma, K.F., Yen, H.Y., Chen, K.S., Chen, Y.I., Lee, C.P. (2006) Precursory phenomena associated with the 1999 Chi–Chi earthquake in Taiwan as identified under iSTEP Program. Physical Chemistry of the Earth, 31, 365–377.

Tsutsui, K., Rokugawa, S., Nakagawa, H., Miyazaki, S., Cheng, C.T., Shiraishi, T. and Yang, S.D. (2007) Detection and volume estimationof large-scale landslides based on elevation-change analysis using DEMs extracted from high-resolution satellite stereo imagery. IEEE Transactions on Geoscience and Remote Sensing, 45, 1681–96.

UN/ISDR (2004) Living with risk: a global review of disaster reduction initiatives. United Nations/International Strategy for Disaster Reduction, Geneva, Switzerland, UN Publications.

USGS (2013) Landsat 8. Available at http://landsat.usgs.gov/LDCM_DataProduct.php Accessed 25 Jun 2013

Van Westen, C.J., Castellanos, E., Kuriakose, S.I. (2008) Spatial data for landslide suscepitibility, hazard, and vulnerability assessment. Engineering Geology, 102, 112-131.

Vu, T.T., Ban, Y. (2010) Context-based mapping of damaged buildings from high-resolution optical satellite images. International Journal of Remote Sensing, 31, 3411–3425.

Vu, T.T., Matsuoka, M., Yamazaki, F. (2004) LiDAR based change detection of buildings in dense urban areas. In: IEEE international geoscience and remote sensing symposium, September 2004, Anchorage, AK, USA, pp 3413–3416.

Wang, F.T., Zhou, Y., Wang, S.X., Liu, W.L., Wei, C.J., Han, Y. (2011) Investigation and assessment of damage in earthquake in Yushu, Qinghai based on multi-spectral remote sensing. Spectroscopy and Spectral Analysis, 31, 1047–1051.

Weston, J., Ferreira, A.M.G., Funning, G.J. (2012) Systematic comparisons of earthquake source models determined using InSAR and seismic data. Tectonophysics, 532–535, 61–81.

Wieland, M., Pittore, M., Parolai, S., Zschau, J., Moldobekov, B., Begaliev, U. (2012) Estimating building inventory for rapid seismic vulnerability assessment: towards an integrated approach based on multisource imaging. Soil Dynamics and Earthquake Engineering, 36, 70–83.

Wurm, M., Taubenböck, H., Dech, S. (2009) Urban structuring using multisensoral remote sensing data. In: Proceedings of the Joint Urban Remote Sensing Event, Shanghai, China, 20-22 May 2009. Shanghai: URS/URBAN.

Zeng, J., Zhu, Z.Y., Zhang, J.L., Ouyang, T.P., Qiu, S.F., Zou, Y., Zeng, T. (2011) Social vulnerability assessment of natural hazards on county-scale using high spatial resolution satellite imagery: a case study in the Luogang district of Guangzhou, South China. Environmental Earth Science, 65, 173–182.